

Supplementary information

Direct synthesis of tetraalkoxysilanes in a high-pressure mechanochemical reactor.

Ilya N. Krizhanovskiy^a, Maxim N. Temnikov^{* a}, Anton A. Anisimov^a, Andrew K. Ratnikov^{a,d}, Ivan Levin^c, Alexander Naumkin, Sergey M. Chistovalov and Aziz M. Muzaferov^{a,b}.

^aA.N. Nesmeyanov Institute of Organoelement Compounds of Russian Academy of Sciences (INEOS RAS) Russia, Vavilova St. 28, Moscow, Russian Federation.

^bEnikolopov Institute of Synthetic Polymeric Materials Russian Academy of Sciences, Moscow, Russia.

^cTopchiev Institute of Petrochemical Synthesis, Russian Academy of Sciences, 29 Leninskii Prospekt, 119991 Moscow, Russia.

^dMendeleev University of Chemical Technology, 9 Miusskaya ploshchad', 125047 Moscow, Russia.

E mail: temnikov88@gmail.com

Contents

Direct synthesis of tetraalkoxysilanes in a high-pressure mechanochemical reactor.....	1
1. SEM-EDX.....	3
2. ^1H , ^{13}C , ^{29}Si NMR – data	4
3. XPS	5
4. Spectra and other additional information	11
4.1. SEM-EDX – images and spectra	11
4.2. NMR	33
4.3. PXRD – date	45
4.4. GLC-MS – spectra.....	49
4.5. XPS – spectra.....	53
5. References.....	68

1. SEM-EDX

Sample	SM-150-15		SM-150-25		SM-150-110				SM-200-15			SM-200-25			SM-200-70			SM-250-15		SM-250-25		SM-250-65			
Elements	1	2	1	2	1	2	3	4	1	2	3	1	2	3	1	2	3	1	2	1	2	1	2	1	2
Si	56.51	65.37	27.97	67.32	83.46	26.99	26.91	83.09	32.46	71.36	2.64	75.89	80.39	14.08	14.37	20.81	14.20	70.01	65.85	2.63	3.86	3.86	3.93		
Cu	36.85	0.80	48.08	0.70	5.05	65.35	65.16	5.03	52.84	0.61	0.38	0.98	0.44	42.69	11.02	13.19	10.87	6.04	5.81	0.38	1.06	0.52			
C	3.62	24.70	19.13	31.56					8.64	21.92	19.78	19.11	18.79	17.59	30.95		29.98	10.60	14.52	19.67	14.71	19.87			
O	1.79	8.75							1.57	5.70	45.46	3.50		9.57					11.76	11.56	45.51	31.00	48.15		
Al	0.77	0.14	1.10	0.24	2.20	2.62	2.61	2.19	0.78	0.14	7.28			1.31	7.23	13.95	7.17	0.24	0.23	7.26	1.96	2.70			
Cl	0.46	0.24	2.16	0.18	3.52	2.56	2.55	3.49	0.83	0.14	9.82	0.19	0.06	1.26	11.23	18.66	11.02	0.63	0.96	9.80	2.70	4.90			
Fe			1.11						0.74	0.13		0.10	0.09	5.58					0.26	0.48		20.65	0.97		
Cr			0.45		5.77	2.48	2.47	5.72	0.31		7.88	0.07	0.04	4.12	25.19	33.40	24.67	0.12		7.87	15.38	12.17			
Ni						0.26	0.33						3.80				1.52			0.02	2.44	0.09			
Ti						0.04	0.15										0.57			0.13	0.67	0.59			
Zn									1.84		6.75	0.16	0.19						0.30	0.59	6.74	2.30	3.18		
Mg																		0.04			3.27	2.93			

Table S1 – SEM-EDX elemental analyses data table

2. ^1H , ^{13}C , ^{29}Si NMR – data

For results of synthesis with methanol

^1H NMR ((CDCl₃, δ, ppm, J/Hz): 3.68 (s, 1H), 3.50 – 3.44 (m, 12H), 3.40 (s, 3H).

^{13}C NMR ((CDCl₃, δ, ppm): 60.14 (s), 50.99 (s), 50.92 (s), 50.87 (s), 50.13 (s).

^{29}Si NMR ((CDCl₃, δ, ppm): -78.72 (s), -86.08 (s).

For results of synthesis with ethanol

^1H NMR ((CDCl₃, δ, ppm, J/Hz): 3.84 (q, J = 7.0 Hz, 2H), 3.70 (q, J = 7.0 Hz, 2H), 2.17 (s, 1H), 1.23 (t, J = 7.0 Hz, 3H), 1.22 (t, J = 7.0 Hz, 3H).

^{13}C NMR ((CDCl₃, δ, ppm): 59.03 (s), 57.64 (s), 17.90 (s), 17.83 (s), 17.75 (s).

^{29}Si NMR ((CDCl₃, δ, ppm): -81.92 (s), -88.97 (s), -89.17 (s).

For results of synthesis with butanol

^1H NMR ((CDCl₃, δ, ppm, J/Hz): 3.78 (t, J = 6.6 Hz, 2H), 3.67 (q, J = 11.4, 6.4 Hz, 2H), 1.61 – 1.54 (m, 4H), 1.49 (t, J = 4.7 Hz, 1H), 1.45 – 1.35 (m, 4H), 0.95 (t, J = 7.4 Hz, 3H), 0.93 (t, J = 7.4 Hz, 3H).

^{13}C NMR ((CDCl₃, δ, ppm): 63.14 (s), 62.19 (s), 34.65 (s), 34.33 (s), 18.83 (s), 18.73 (s), 13.70 (s), 13.63 (s).

^{29}Si NMR ((CDCl₃, δ, ppm): -81.84 (s), -88.84 (s).

For results of synthesis with ethoxyethanol

^1H NMR ((CDCl₃, δ, ppm, J/Hz): 3.94 (t, J = 5,5 Hz, 2H), 3.76 – 3.72 (m, 2H), 3.58 – 3.50 (m, 8H), 2.39 (s, 1H), 1.23 (t, J = 7.0 Hz, 3H), 1.19 (t, J = 7.0 Hz, 3H).

^{13}C NMR ((CDCl₃, δ, ppm): 71.69 (s), 71.15 (s), 66.39 (s), 66.30 (s), 62.77 (s, J = 6.1 Hz), 61.44 (s), 14.98 (s), 14.89 (s).

^{29}Si NMR ((CDCl₃, δ, ppm): -82.49 (s), -89.17 (s).

3. XPS

Spent mass	Elements, at%							
	C	O	Si	Cl	Cr	Cu	Zn	F
SM150	39.4	40.3	12.0	1.5	4.8	1.1	1.0	-
SM200-15	23.5	36.9	33.9	1.6	0.7	2.6	0.8	-
SM200-25	30.7	36.4	24.5	2.7	0.8	3.4	1.5	-
SM200	47.2	41.0	2.1	1.7	6.4	0.7	0.9	-
SM250	52.6	35.6	1.8	1.4	7.2	0.5	0.9	2.7

Table S2. Concentrations of elements on the surface of the studied samples (atom. %), calculated from the survey XPS spectra.

Spent mass	Elements, at%								
	C	O	Si	Si ⁰	Si ⁴⁺	Cl	Zn	Cr	Cu
SM150	42.7	39.0	13.0	10.4	2.6	1.5	1.0	4.3	1.0
SM200-15	26.9	34.5	35.9	28.0	7.9	1.6	0.8	0.6	2.2
SM200-25	33.2	35.1	27.4	19.2	8.2	2.7	1.5	1.0	3.3
SM200	52.0	39.3	2.4	0.6	1.8	1.7	0.9	5.9	0.6
SM250	56.1	35.1	2.0	0	2.0	1.2	0.9	6.7	0.1

Table S3 - Concentrations of elements on the surface of the studied samples (atom. %), Calculated from the high-resolution XPS spectra.

Sample	Oxidation state	Si ⁰		Si ⁴⁺
		Peak 2p _{3/2} , eV	2p _{1/2} , eV	2p _{3/2} , eV
SM-150	BE, eV	99.34	99.95	103.4
	W, eV	0.93	1.12	2.08
	I _{relative}	0.53	0.27	0.20
SM-200-15	BE, eV	99.34	99.95	103.44
	W, eV	0.77	0.82	1.90
	I _{relative}	0.52	0.26	0.22
SM-200-25	BE, eV	99.34	99.95	103.34
	W, eV	0.89	1.08	1.98
	I _{relative}	0.47	0.23	0.30
SM-200	BE, eV	99.34	99.95	103.44
	W, eV	1.06	1.2	2.04
	I _{relative}	0.16	0.08	0.76
SM-250	BE, eV	99.14	99.75	103.44
	W, eV	0.8	1.06	2.03
	I _{relative}	0.026	0.013	0.961

Table S4. Characteristics of photoelectron spectra: binding energies BE, widths (W), and relative intensities (I_{relative}) of photoelectron peaks assigned to different chemical charge states in the Si 2p spectra.

Samples	Parameters	Cu ⁰	Cu ²⁺ ,	Cu ²⁺ , sat1	Cu ²⁺ , sat2	Cu ²⁺ , sat3	Cu ²⁺ , sat4
		I	II	III	IV	V	VI
SM-150	BE	933.2	933.8	935.7	941.7	942.9	944.9
	W	1.5	2.1	3.2	1.0	3.5	1.8
	I _{relative}	0.1	0.3	0.4	0	0.2	0.1
SM-200-15	BE	932.7	934.6	936.0	-	942.3	944.2
	W	1.6	1.7	2.3	-	3.5	1.8
	I _{relative}	0.7	0.1	0.1	-	0.02	0.02
SM-200-25	BE	932.8	934.5	936.0	941.3	942.2	944.0
	W	1.6	1.7	2.3	1.0	3.5	1.8
	I _{relative}	0.7	0.1	0.1	0	0.04	0.03
SM-200	BE	933.2	934.3	935.9	-	942.7	944.8
	W	1.4	2.1	2.1	-	3.5	1.8
	I _{relative}	0.5	0.2	0.2	-	0.1	0.04
SM-250	BE	933.0	934.7	936.1	-	-	-
	W	1.5	1.7	2.3	-	-	-
	I _{relative}	0.8	0.1	0.1	-	-	-

Table S5. Characteristics of photoelectron peaks identified in the Cu 2p_{3/2} spectra: binding energies BE, widths (W), and relative intensities (I_{relative})

Sample	Cu 2p _{3/2} , eV	Cu L ₃ M _{4,5} M _{4,5}	Cu 2p _{3/2} + Cu L ₃ M _{4,5} M _{4,5} , eV	Charge reference, eV	C 1s, eV	Ref.
SM-200	933.2	914.8	1848.0	Si 2p		
	934.3		1849.1	99.34		
SM-150	933.2	915.1	1848.3	Si 2p		
	933.8		1848.9	99.34		
SM-250*						
SM-200-15	932.7	915.9	1848.6	Si 2p 99.3	285.3	
SM-200-25			1848.3			
	932.8	915.5	1850.7	Si 2p	285.2	
	934.4		1849.9	99.3		
			1852.3			
CuCl	932.5	914.9	1847.4		285.0	[1]
CuCl	932.54	914.98	1847.51		285.0	[2]
Cu ₂ O	932.9	916.5	1849.4		285.0	[3]
Cu ₂ O	932.38	916.79	1849.17		285.0	[2]
Cu ₂ O	932.9	916.6	1849.5		285.0	[4]
Cu ₂ O	932.8	915.9	1848.7		285.0	[5]
Cu	932.67	918.49	1851.16	Au 4f _{7/2} 83.98		[6]
Cu(OH) ₂	934.2	916.5	1850.7		285.0	[7]
Cu(OH) ₂	934.87	916.05	1850.92		285.0	[2]
CuCl ₂	935.1	915.3	1850.4		285.0	[8]
CuCl ₂	935.5	914.88	1850.37		285.0	[2]
CuO	933.75	917.7	1851.45		285.0	[9]
CuO	933.77	917.37	1851.33		285.0	[2]

Table S6. Characteristics of photoelectron and Auger spectra of Cu studied samples and reference data.

* Due to the low copper concentration in the sample, a low signal intensity was observed in the region of the Cu-LMM Auger transitions, which made it impossible to determine the E_{kin} of the Auger peak

Sample	Cr 2p _{3/2} , eV	Cr 2p _{1/2} , eV	Cr 2p _{1/2} - 2p _{3/2} , eV	Cu/Cr	Ref.
SM-150	577.9	587.7	9.8	0.24	
SM-200-15	577.6	587.8	10.2	3.84	
SM-200-25	577.3	587.3	10.0	3.39	
SM-200	577.2	587.1	9.9	0.09	
SM-250	576.9	586.6	9.7	0.01	
Cr ₂ O ₃	576.9	586.7	9.8		[10]

Table S7. Characteristics of the Cr 2p photoelectron spectra.

4. Spectra and other additional information

4.1. SEM-EDX – images and spectra

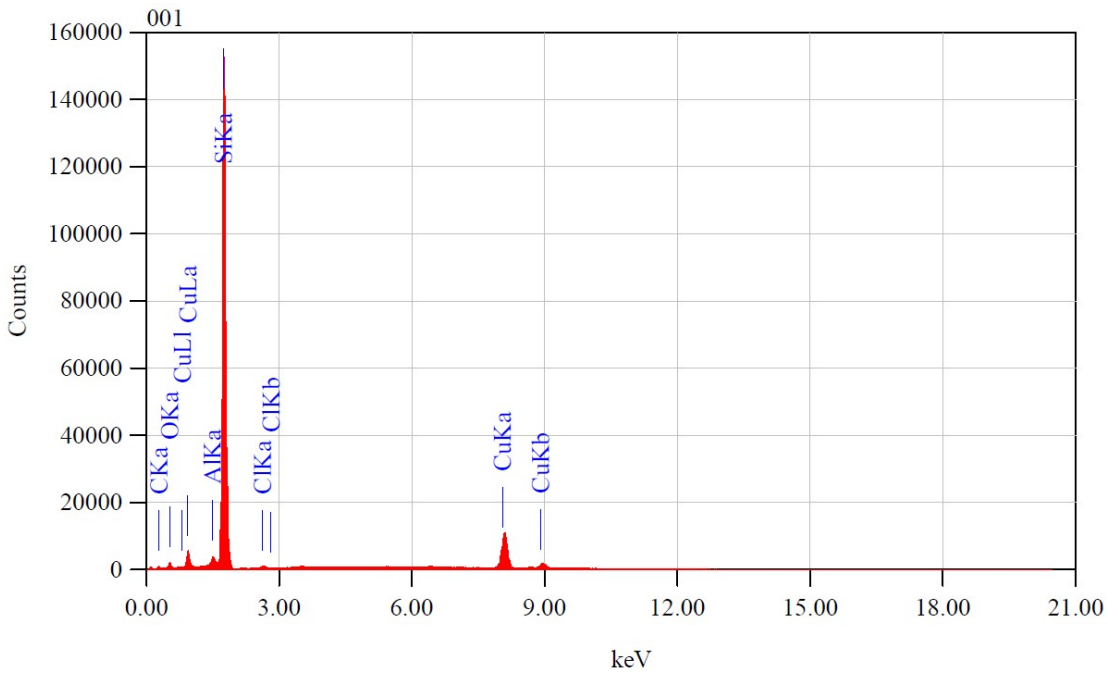
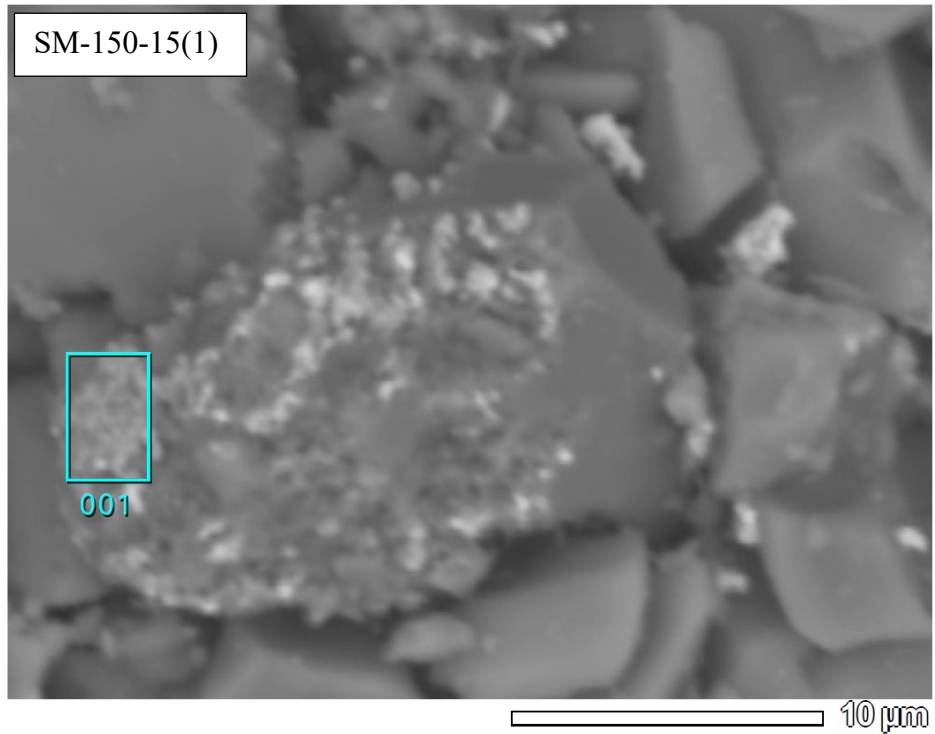


Figure S1 SM-150-15(1)

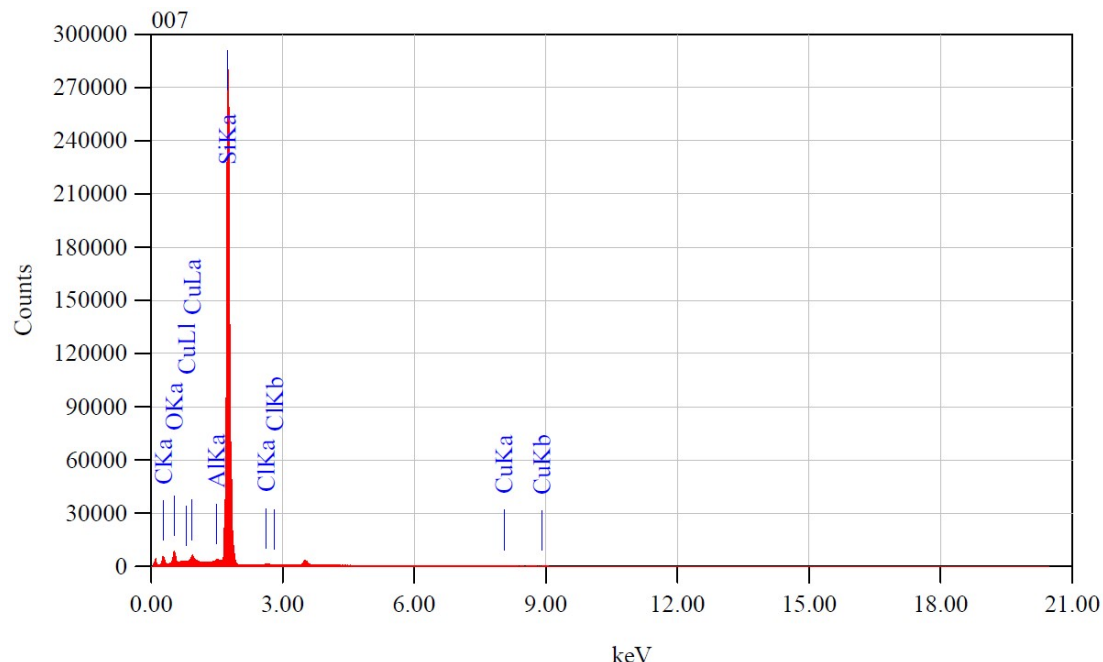
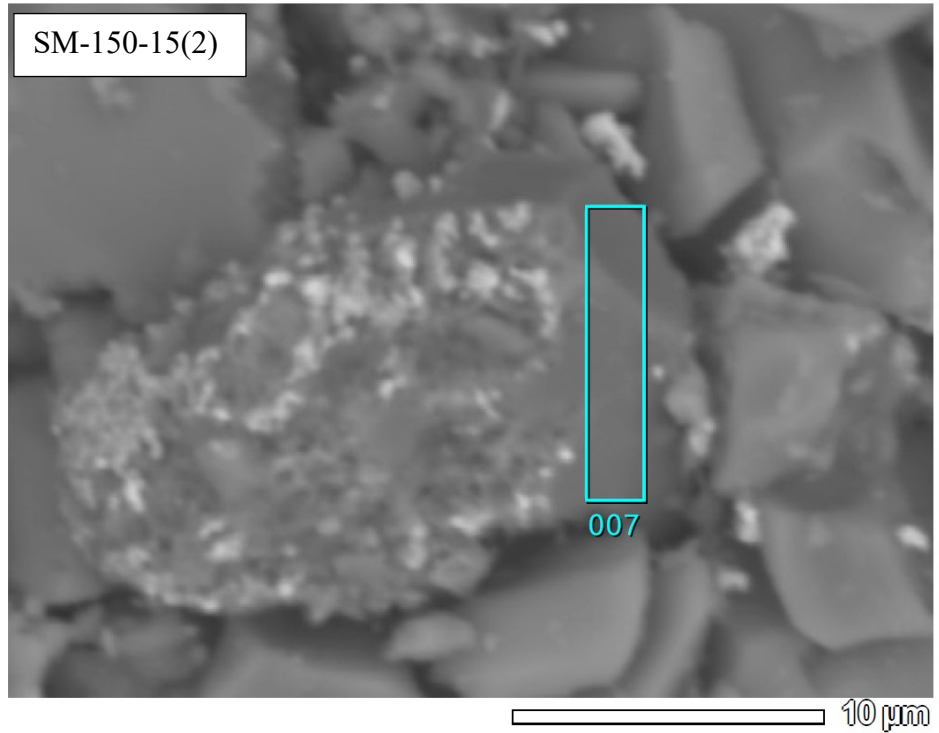


Figure S2 SM-150-15(2)

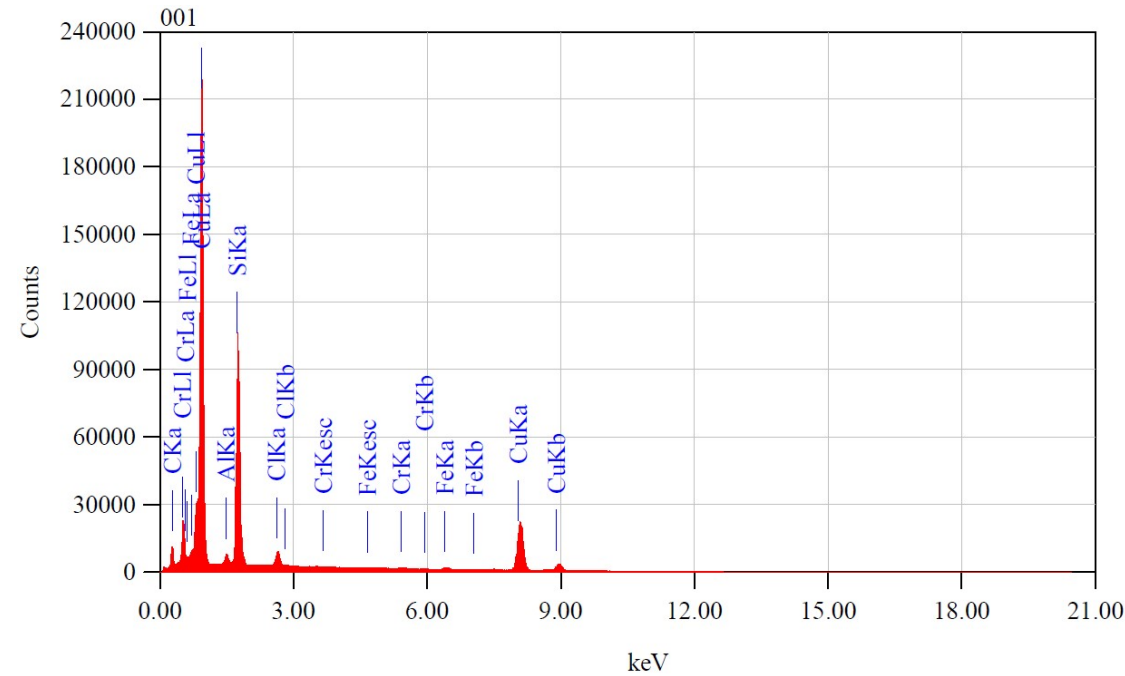
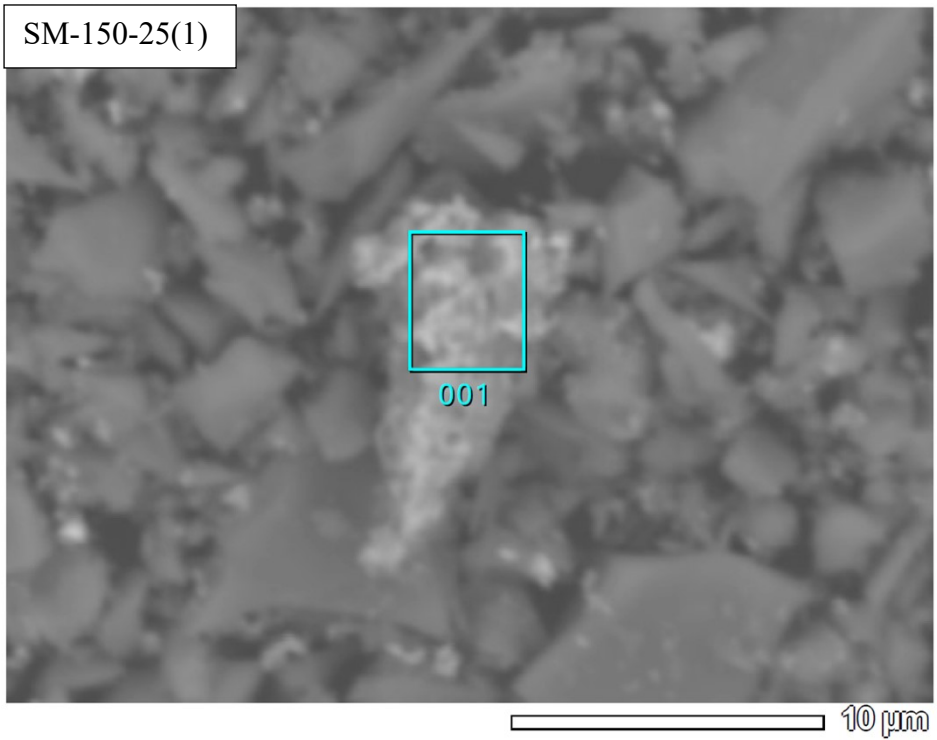


Figure S3 SM-150-25(1)

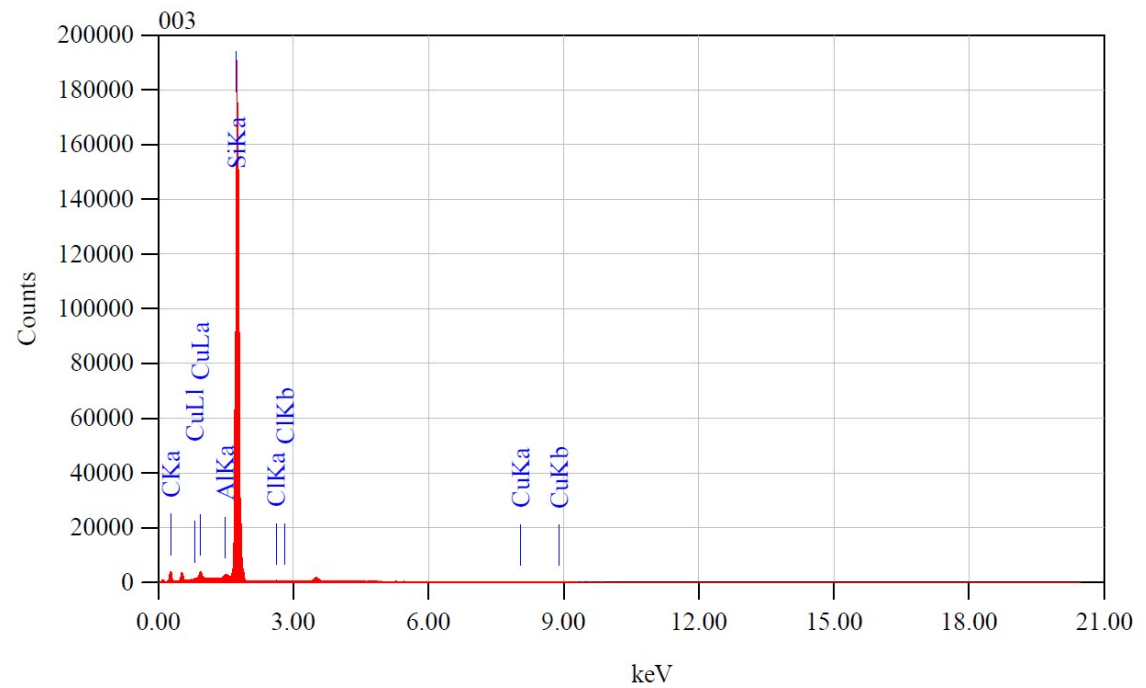
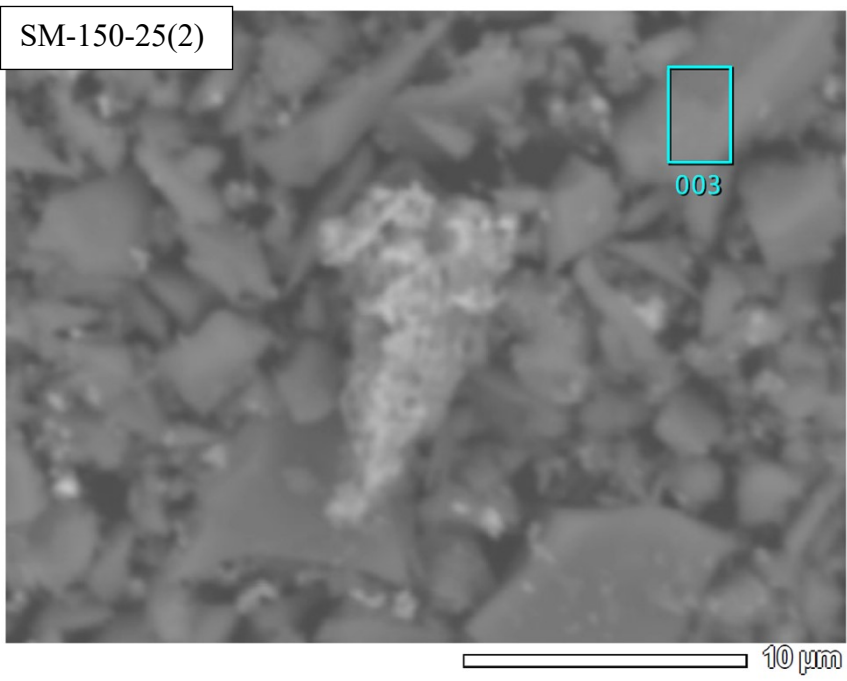


Figure S4 SM-150-25(2)

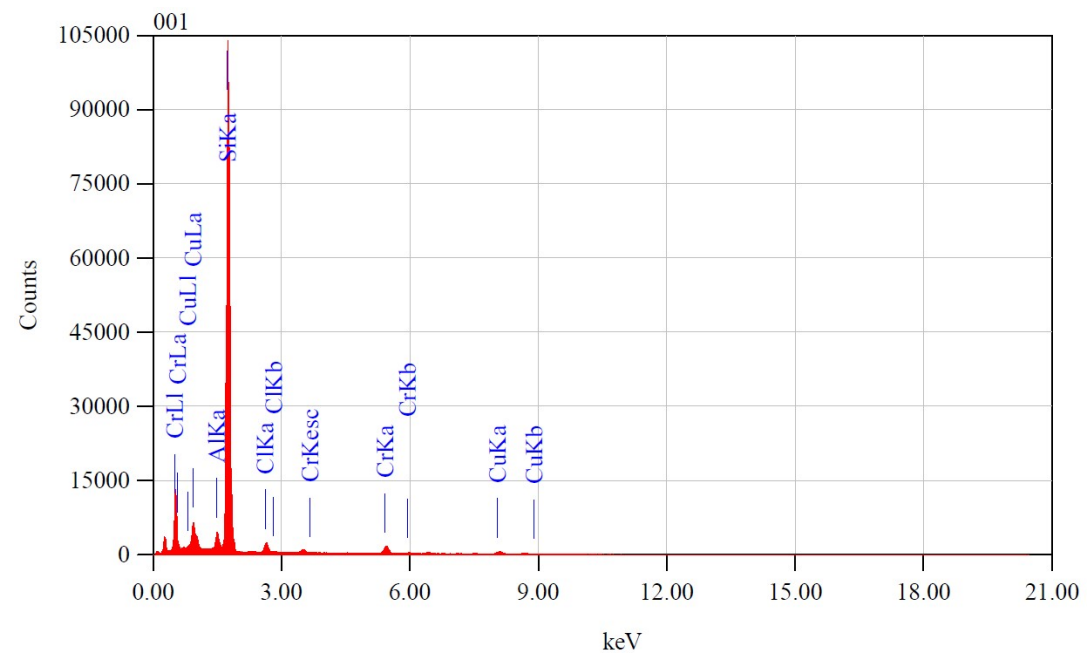
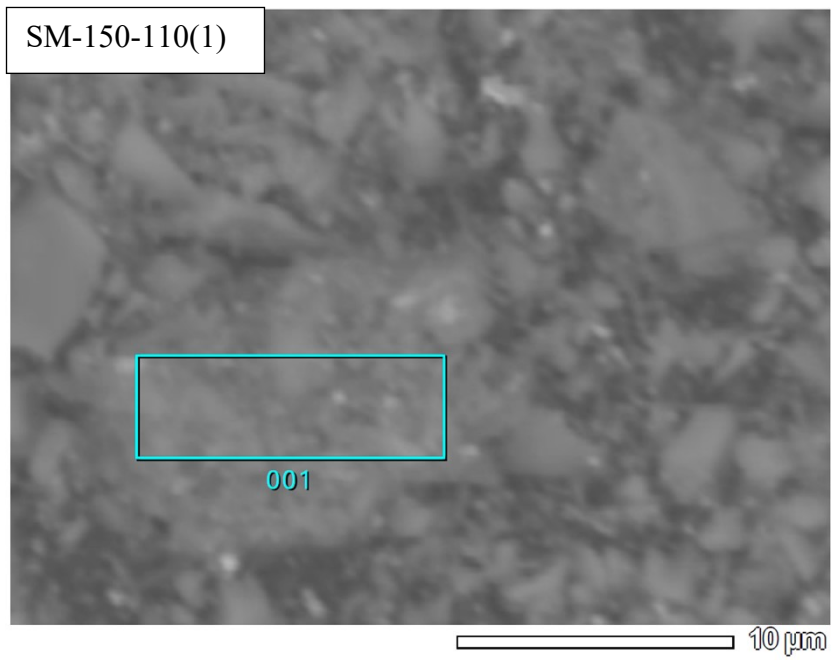


Figure S5 SM-150-110(1)

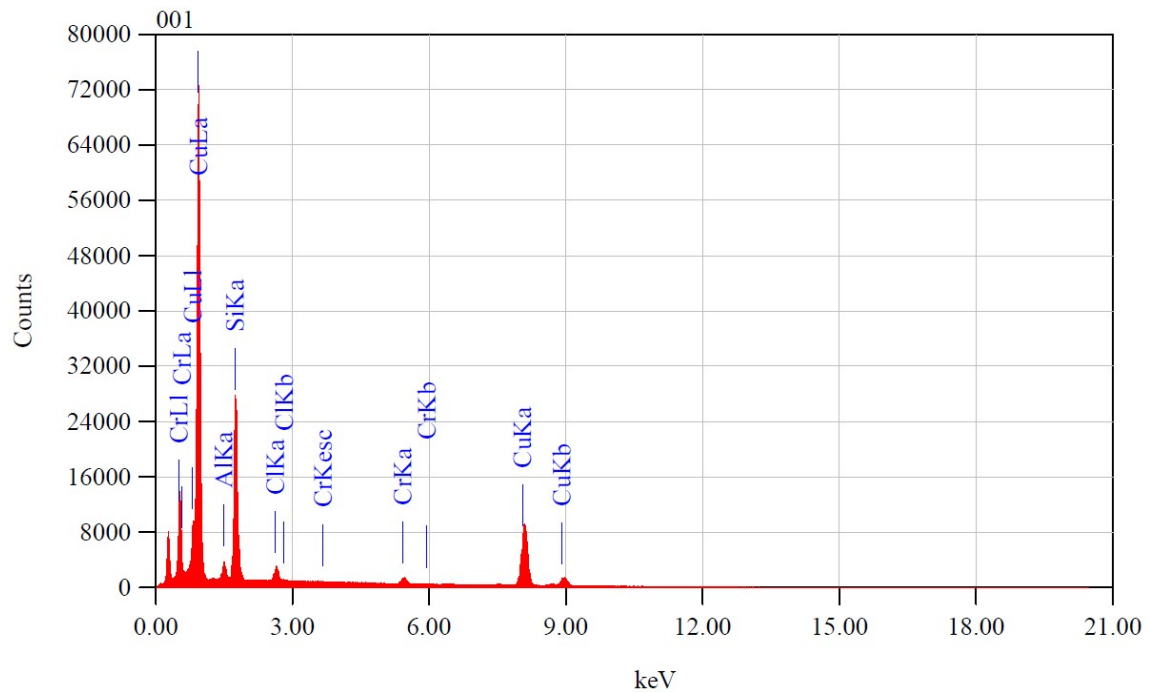
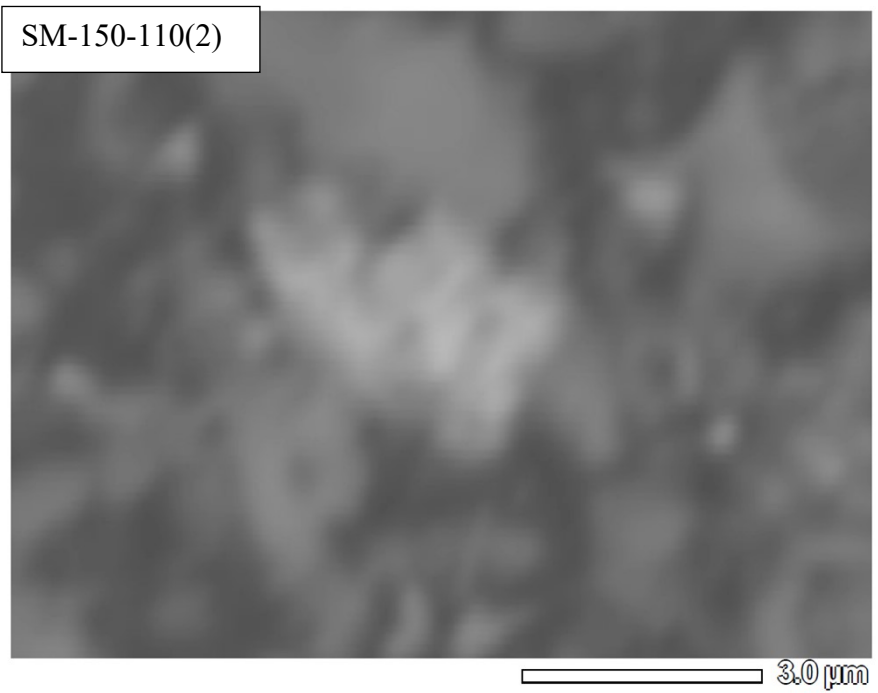


Figure S6 SM-150-110(2)

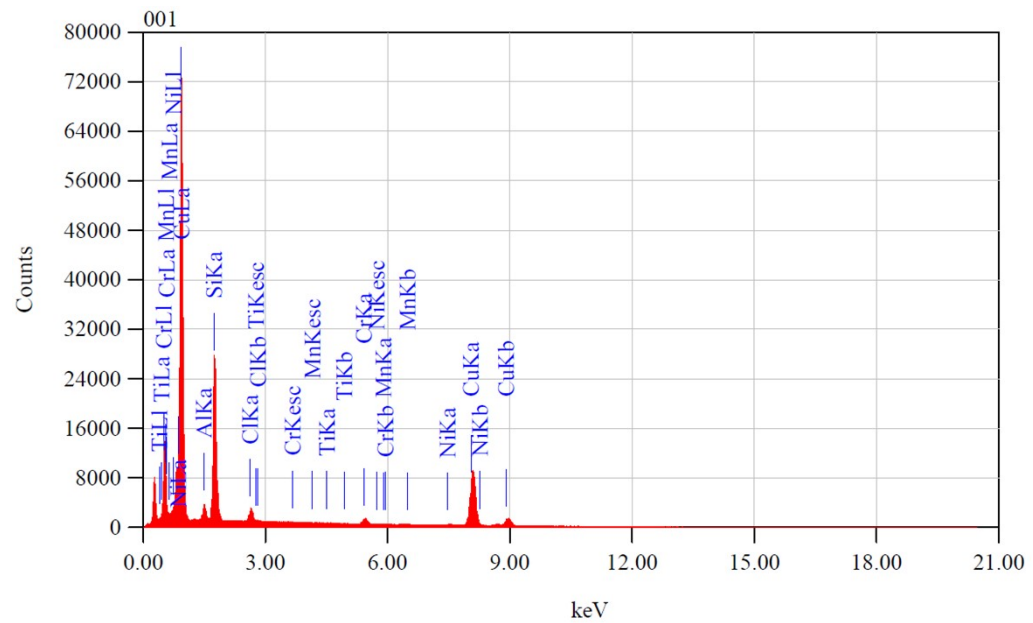
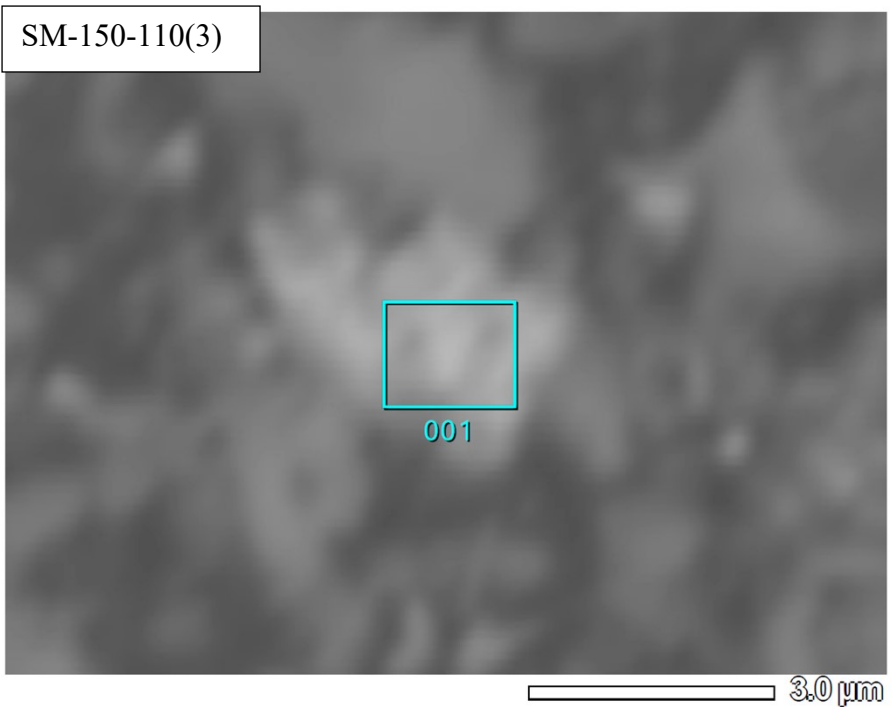


Figure S7 SM-150-110(3)

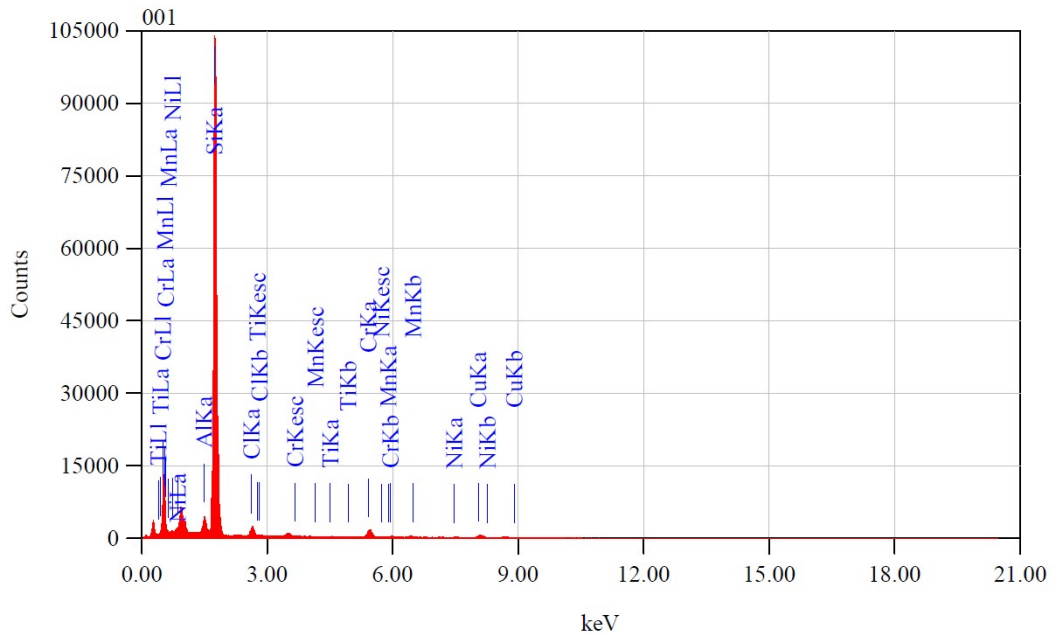
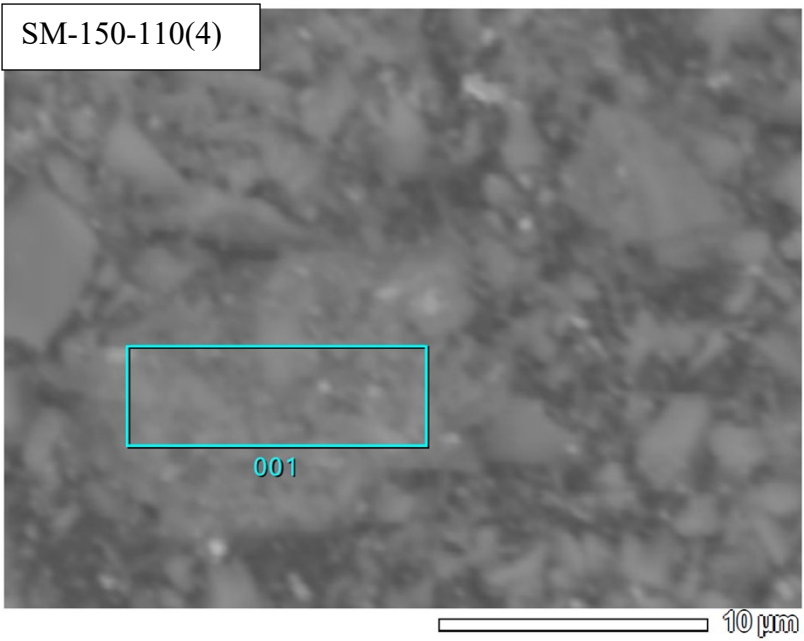


Figure S8 SM-150-110(4)

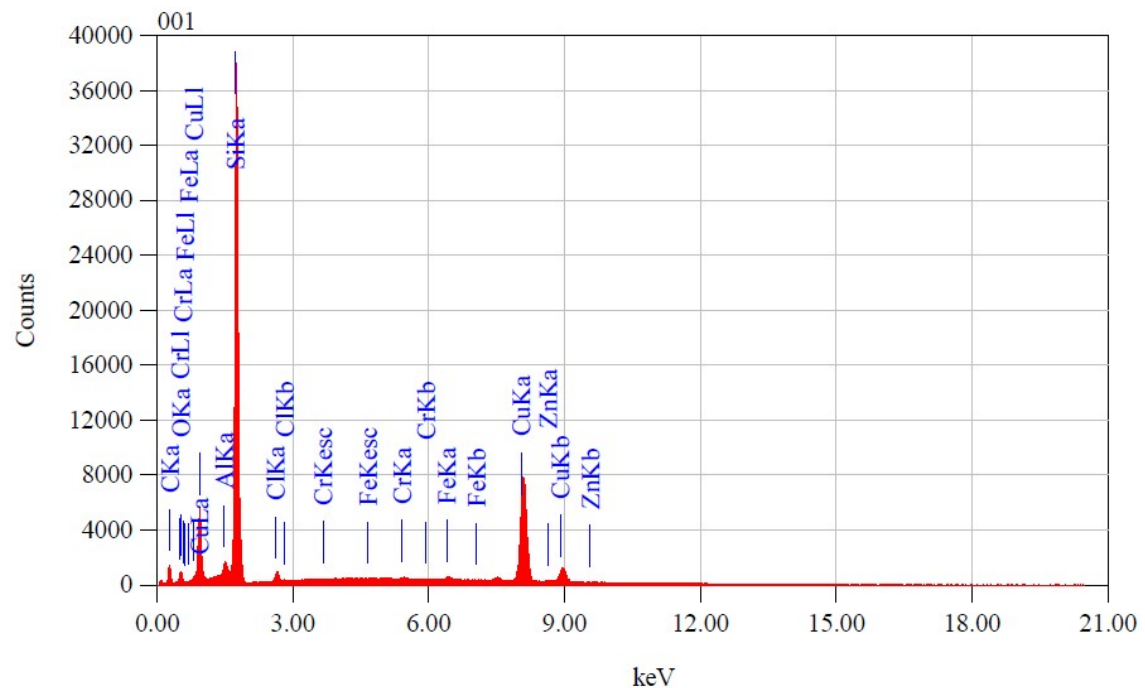
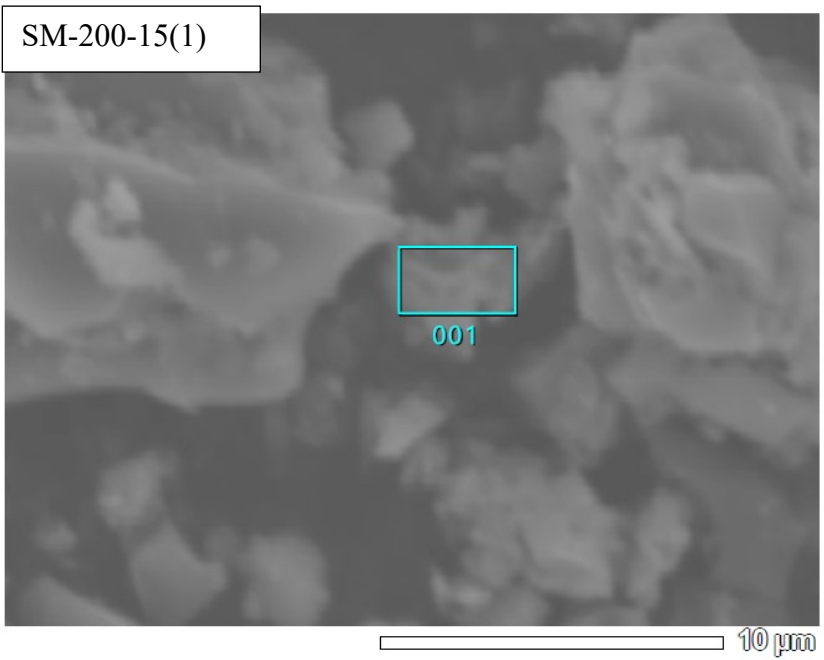


Figure S9 SM-200-15(1)

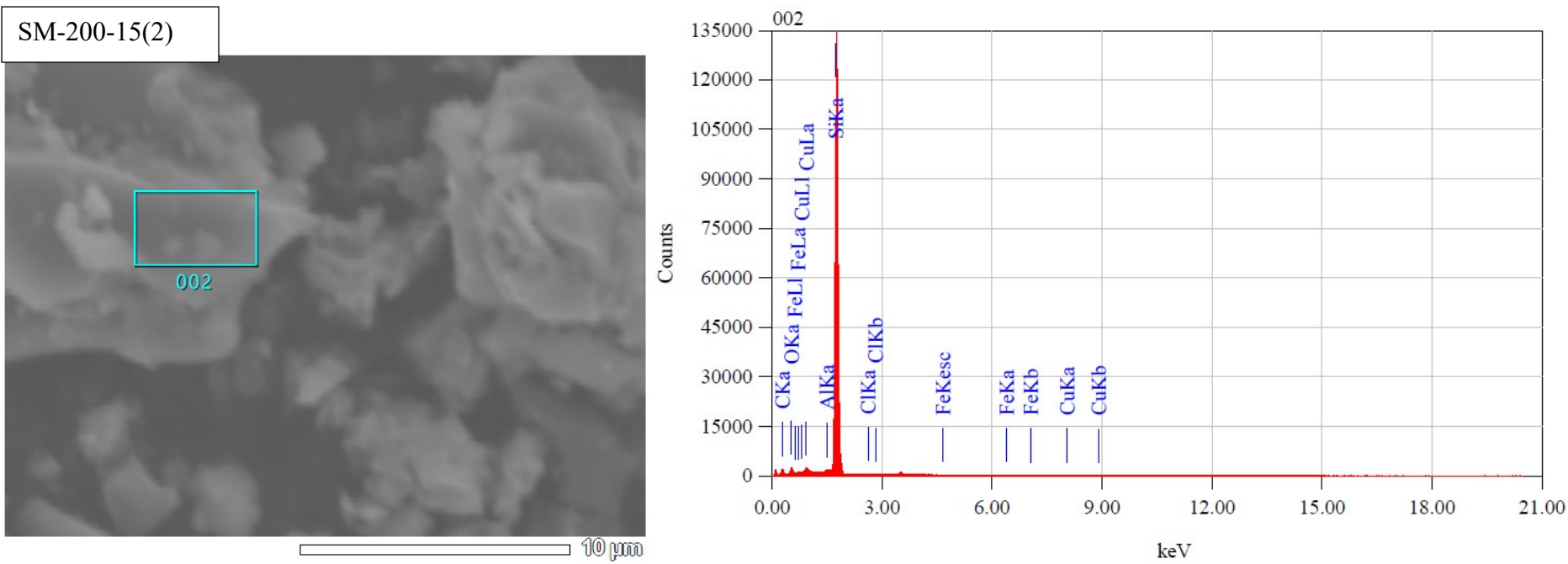


Figure S10 SM-200-15(2)

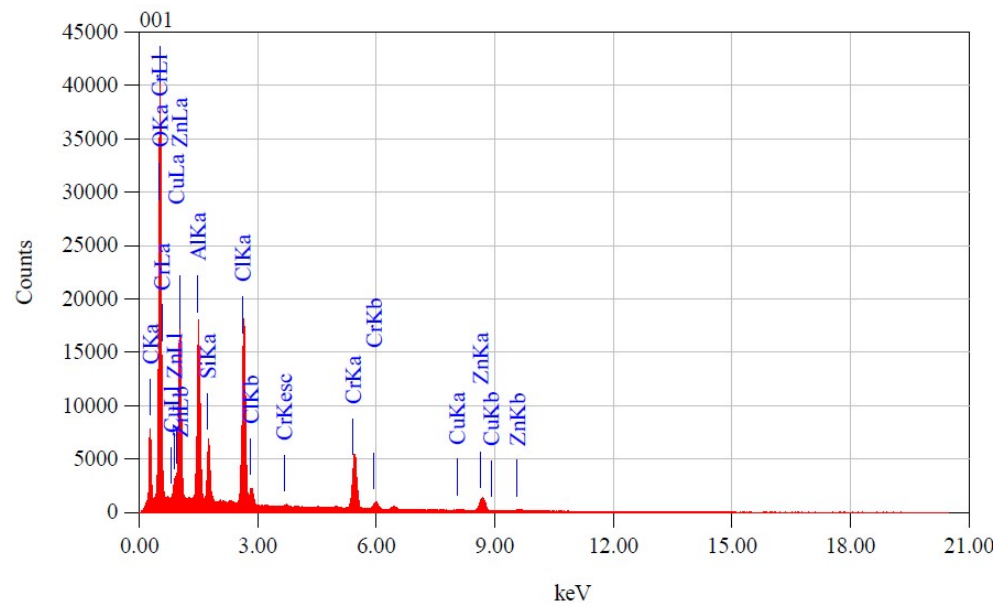
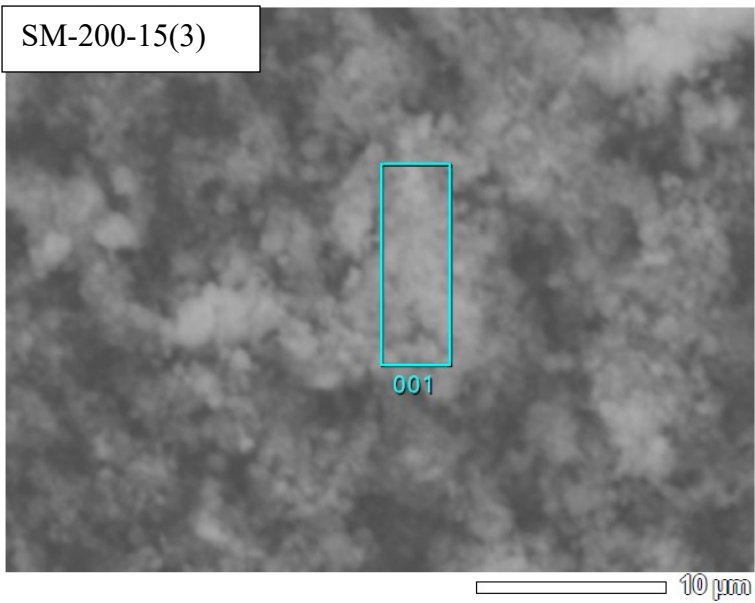


Figure S11 SM-200-15(3)

SM-200-25(1)

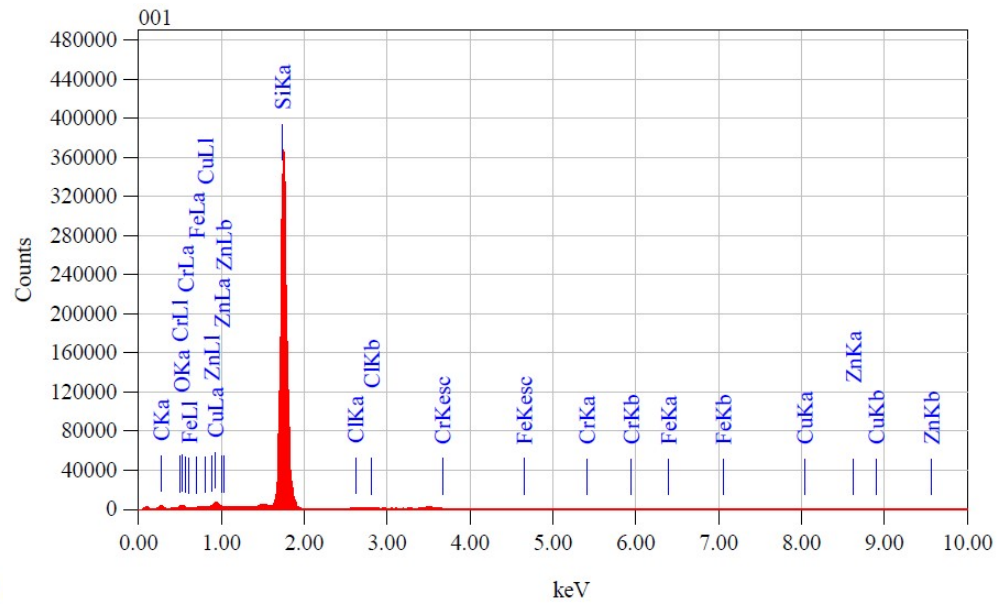
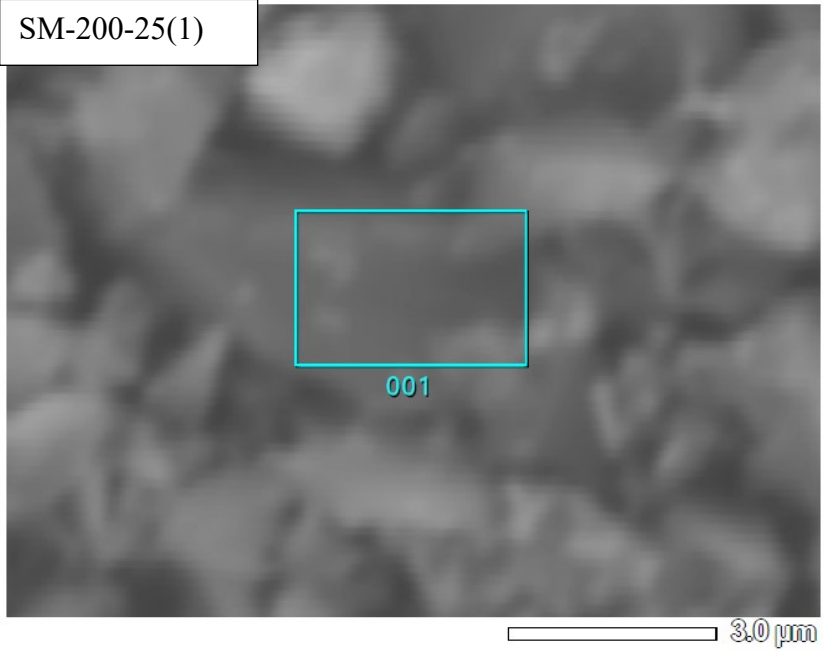


Figure S12 SM-200-25(1)

SM-200-25(2)

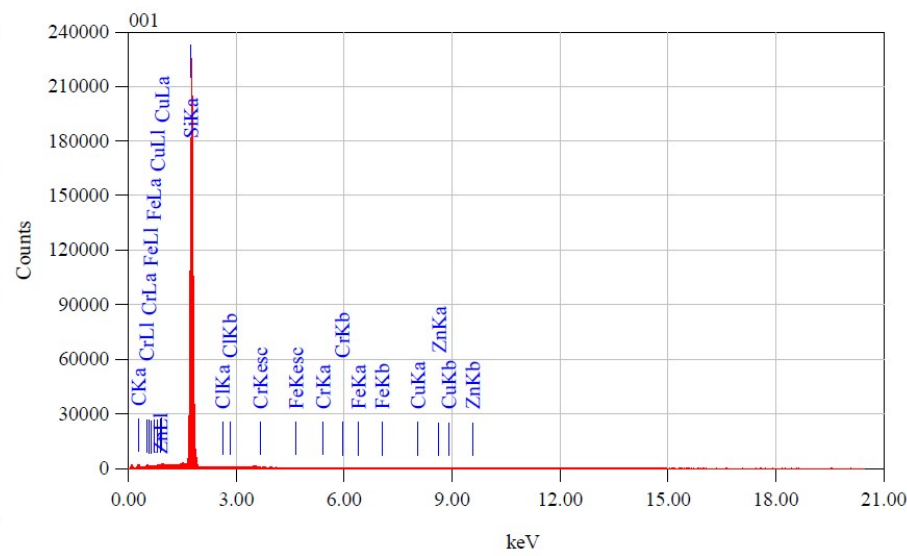
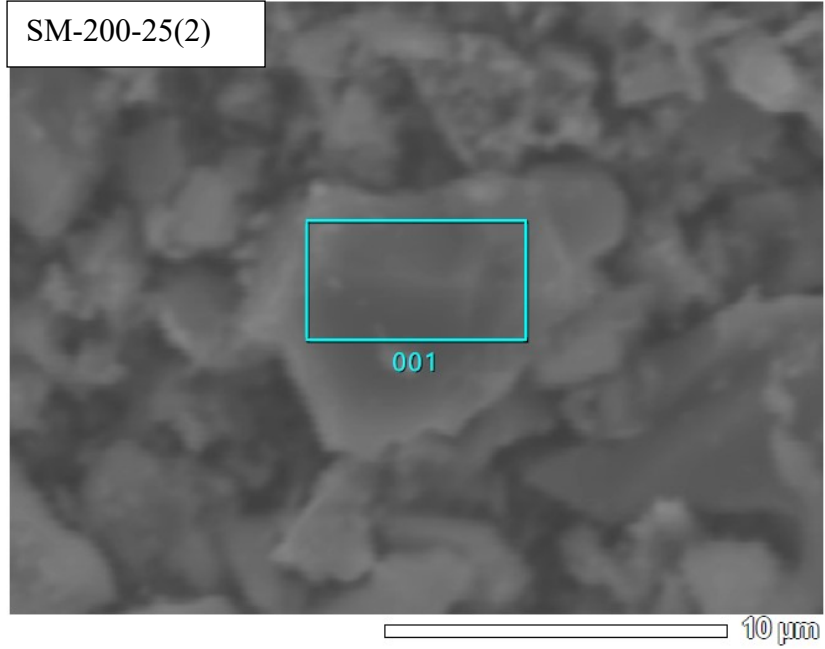


Figure S13 SM-200-25(2)

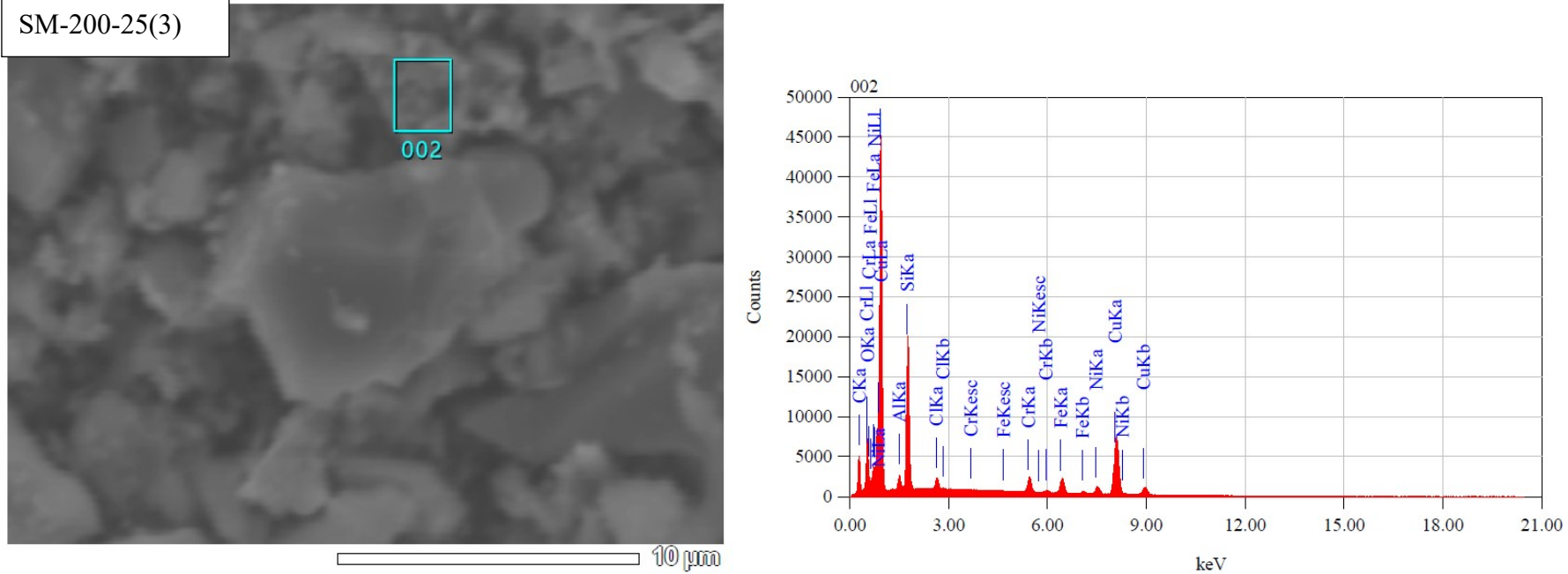


Figure S14 SM-200-25(3)

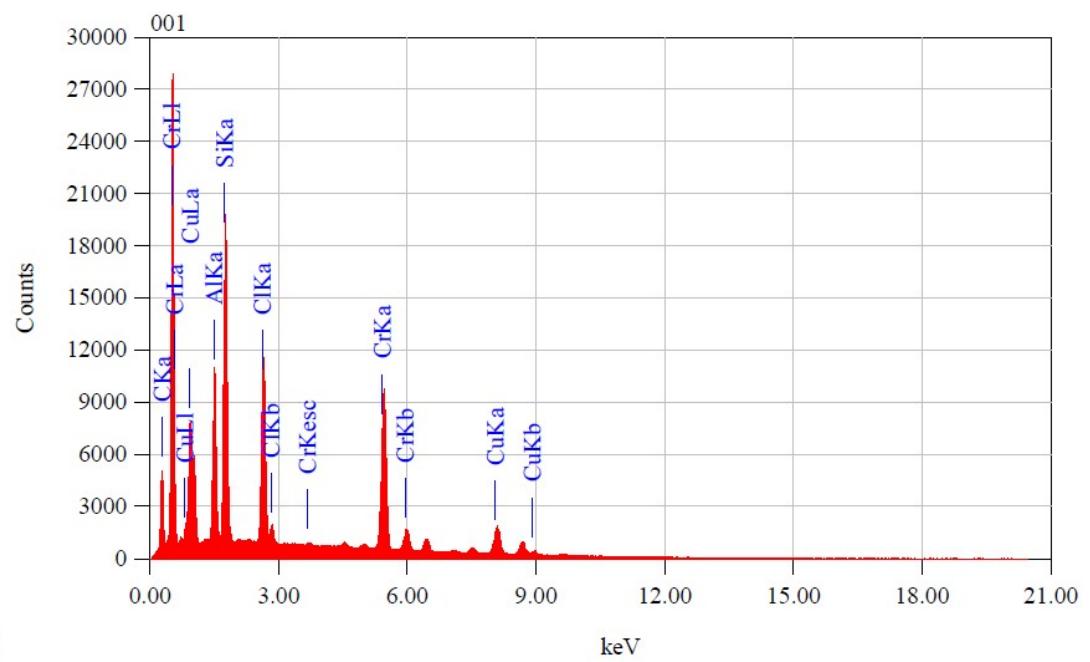
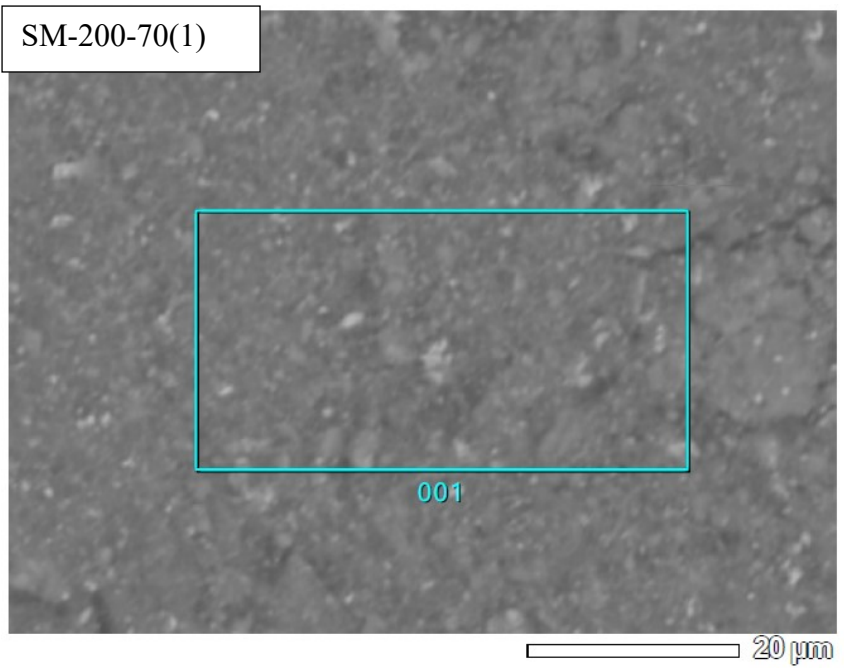


Figure S15 SM-200-70(1)

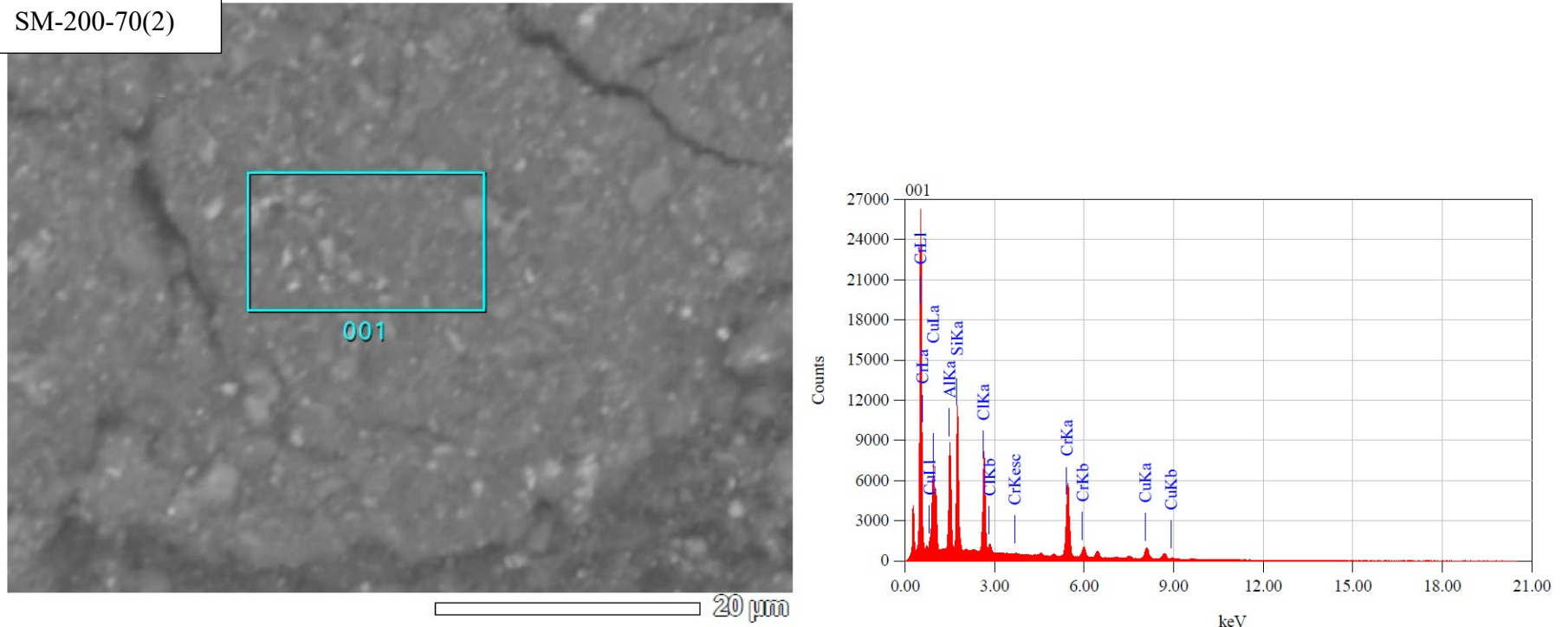


Figure S16 SM-200-70(2)

SM-200-70(3)

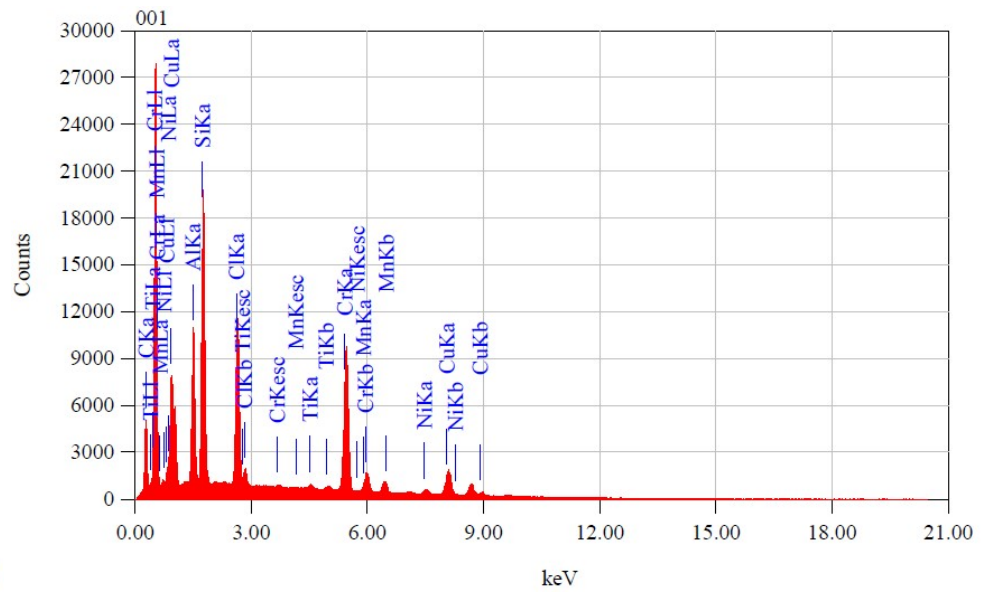
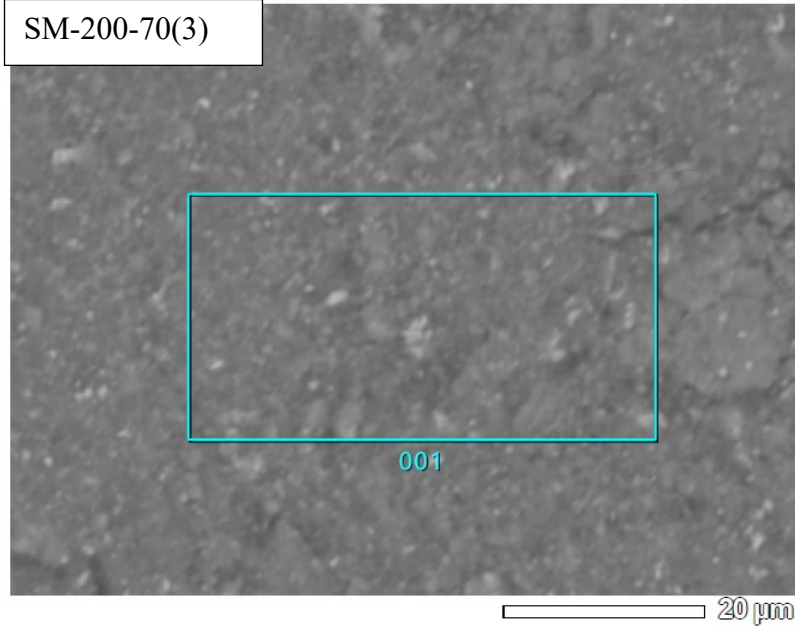


Figure S17 SM-200-70(3)

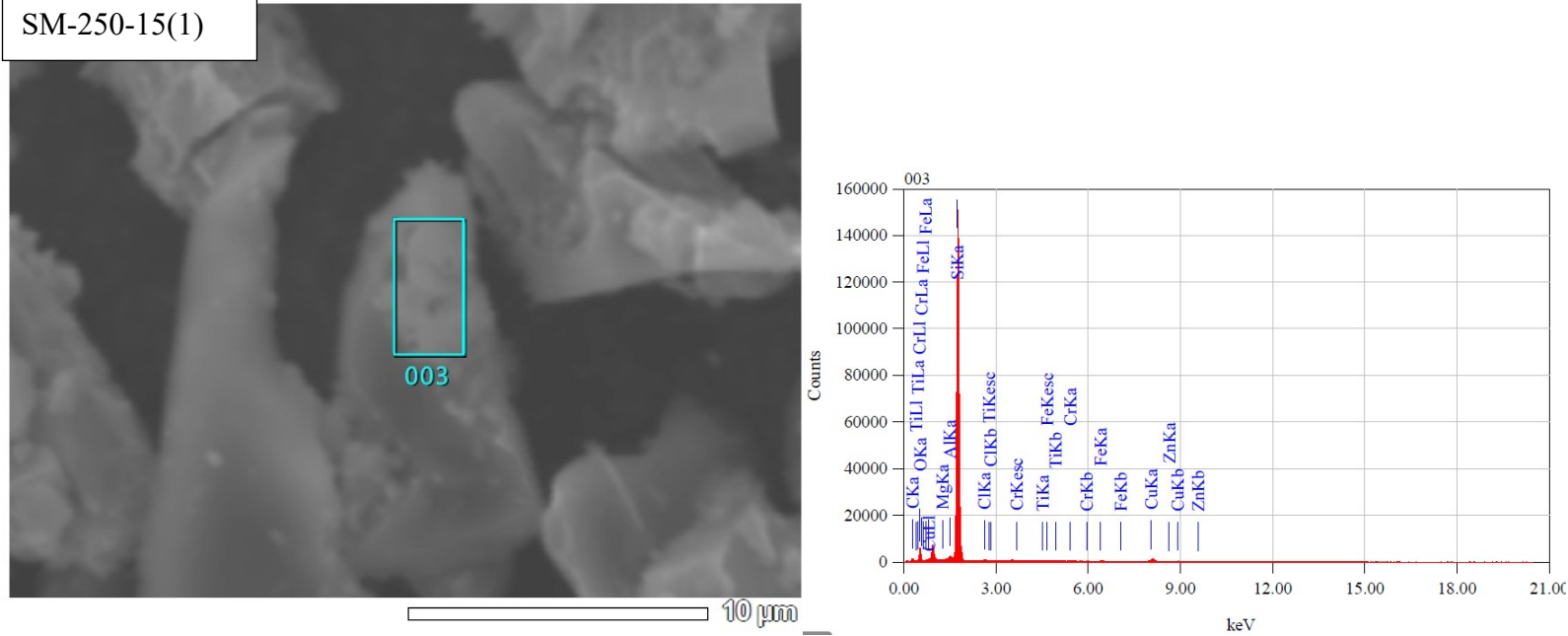


Figure S18 SM-250-15(1)

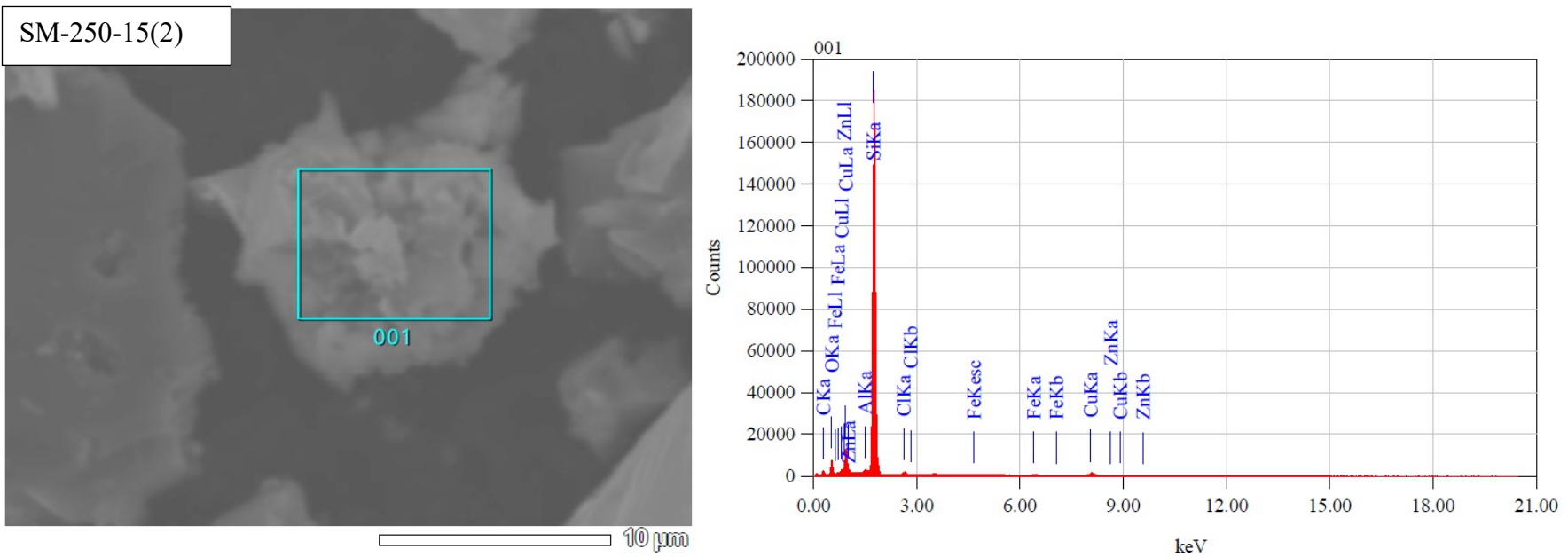


Figure S19 SM-250-15(2)

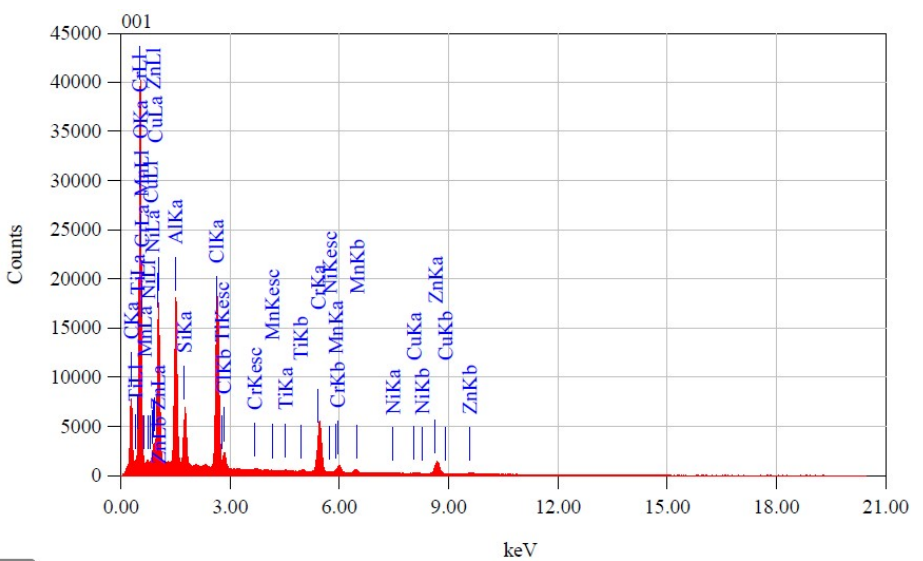
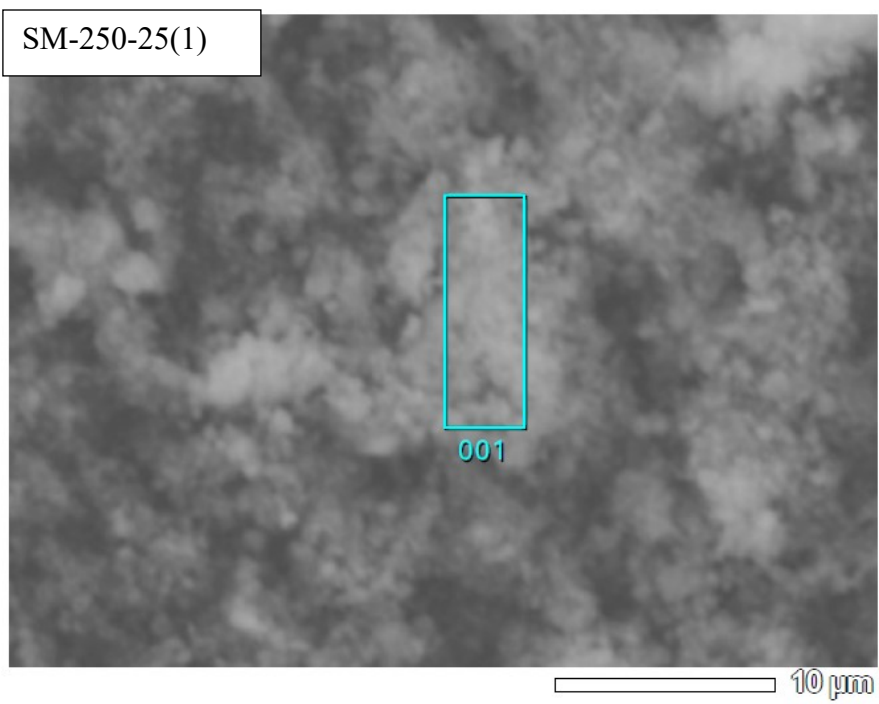


Figure S20 SM-250-25(1)

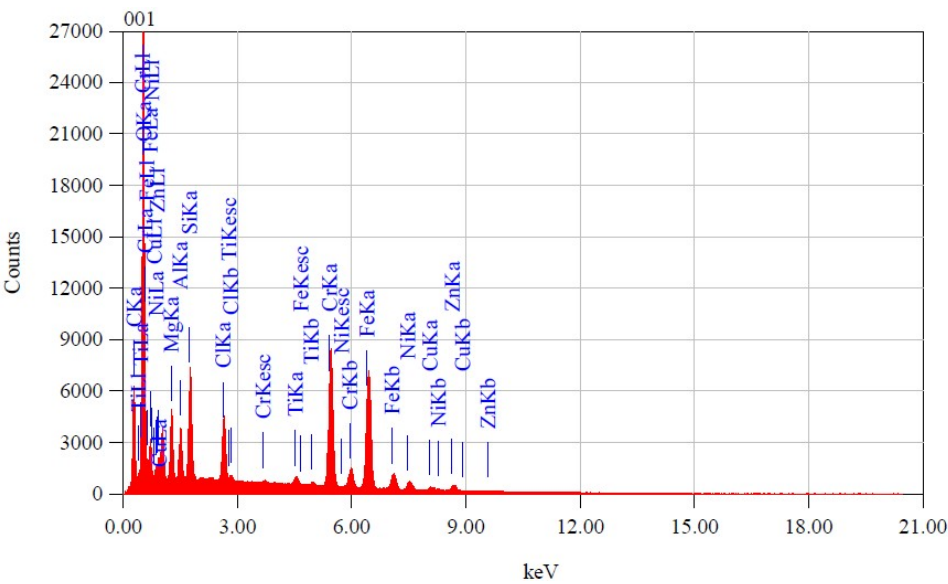
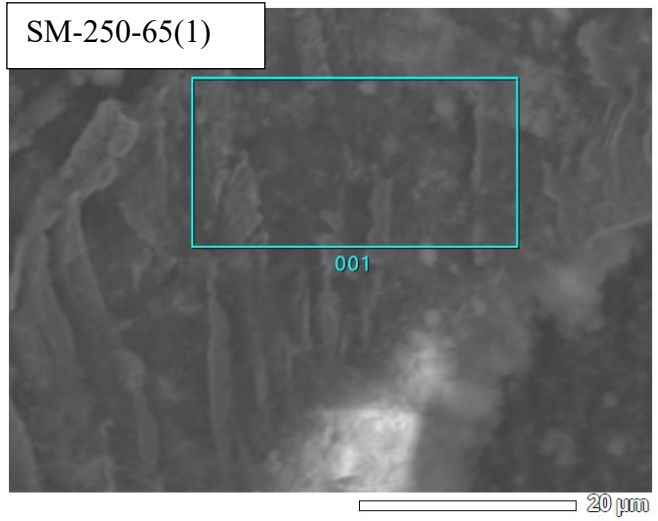


Figure S21 SM-250-65(1)

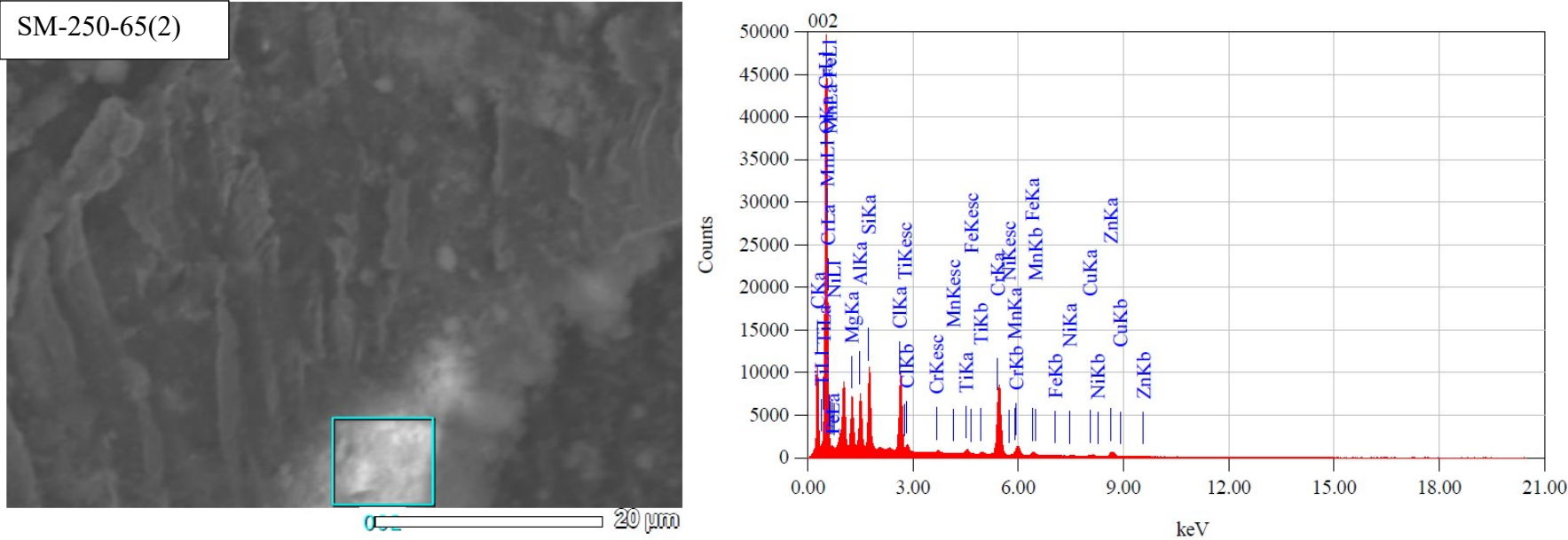


Figure S22 SM-250-65(2)

4.2. NMR

NMR for tetramethoxysilane synthesis

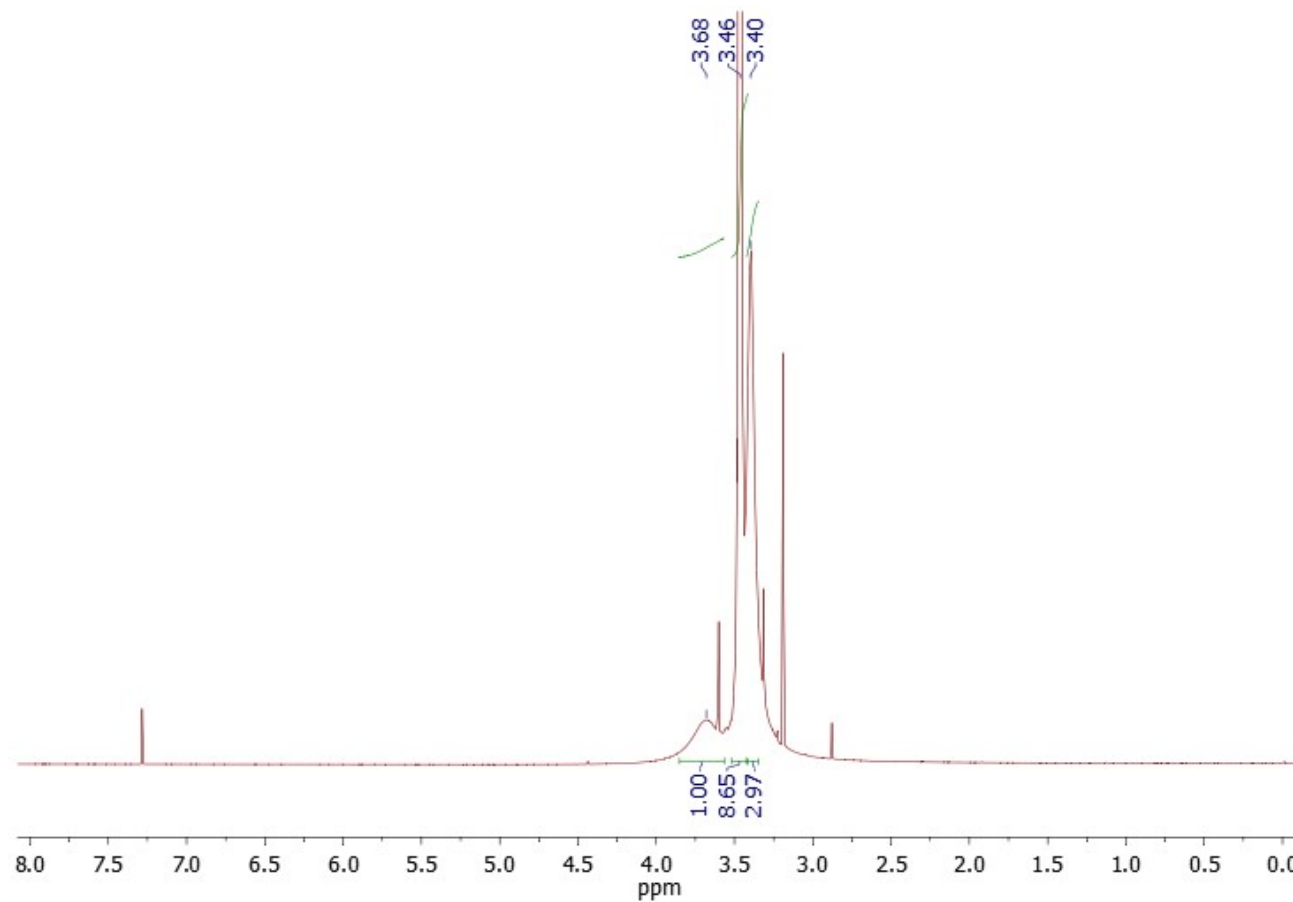


Figure S23 ¹H NMR spectrum for synthesis with methanol

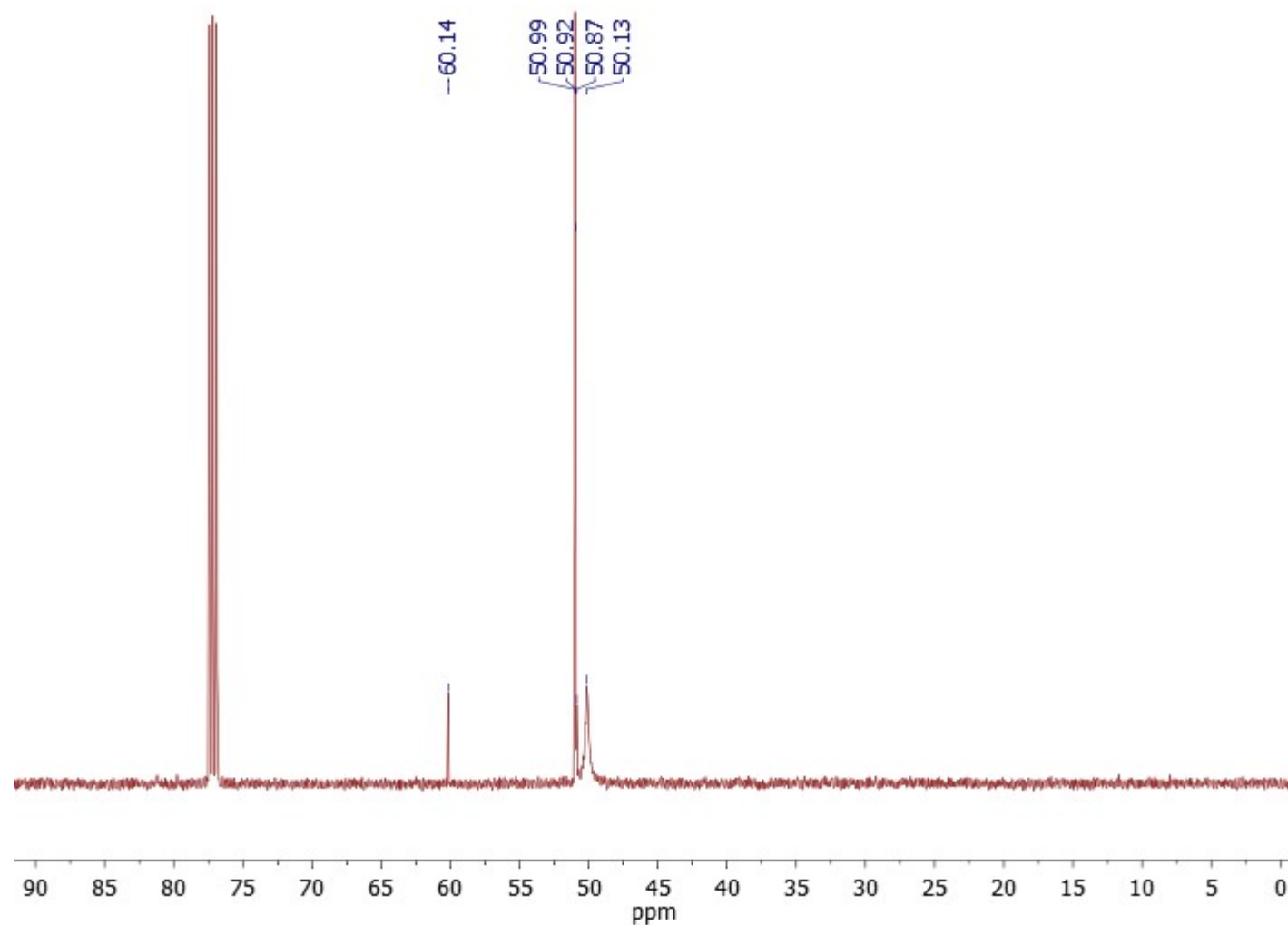


Figure S24 ^{13}C NMR spectrum for synthesis with methanol

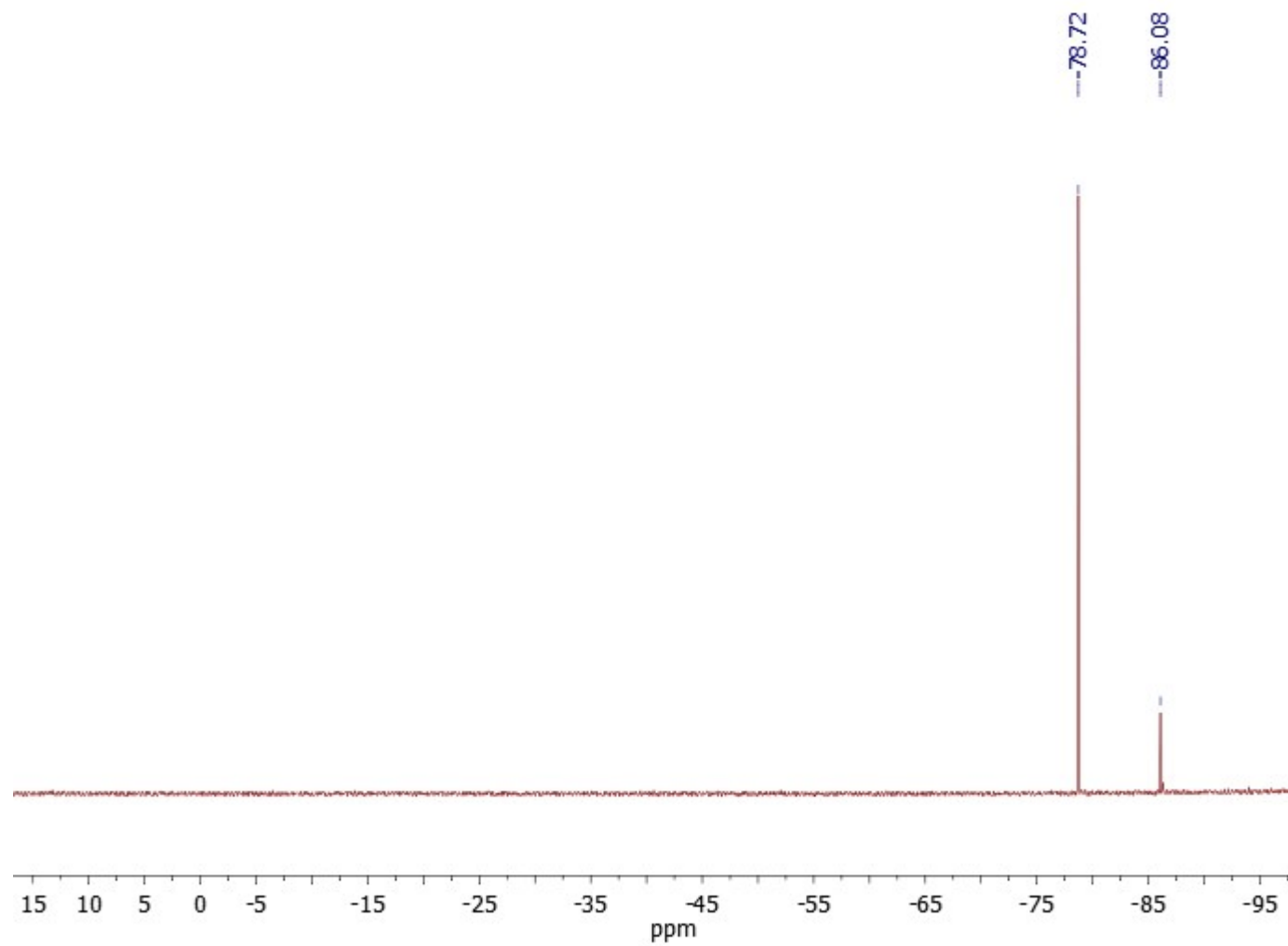


Figure S25 ^{29}Si NMR spectrum for synthesis with methanol

NMR for tetraethoxysilane synthesis

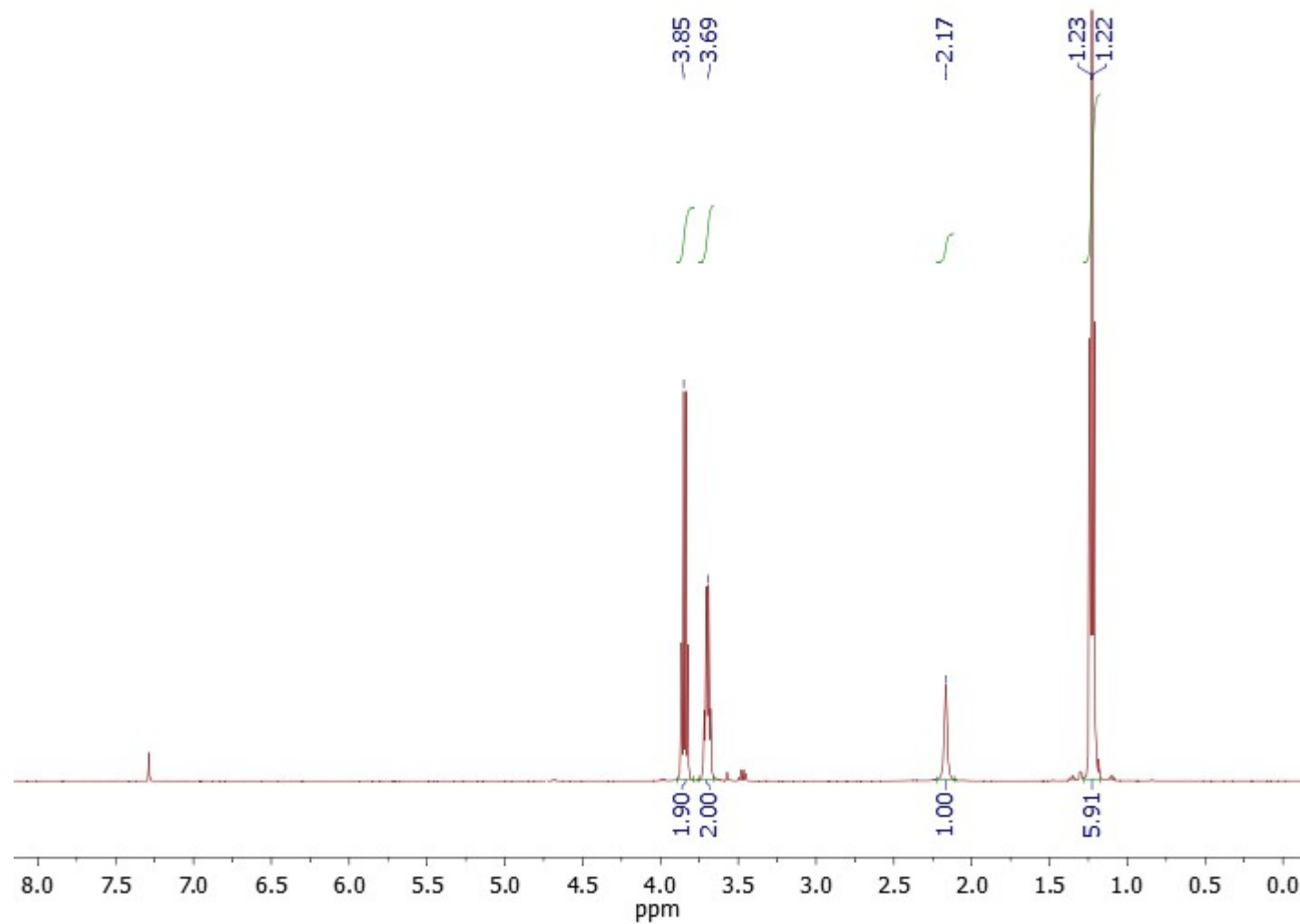


Figure S26 ¹H NMR spectrum for synthesis with ethanol

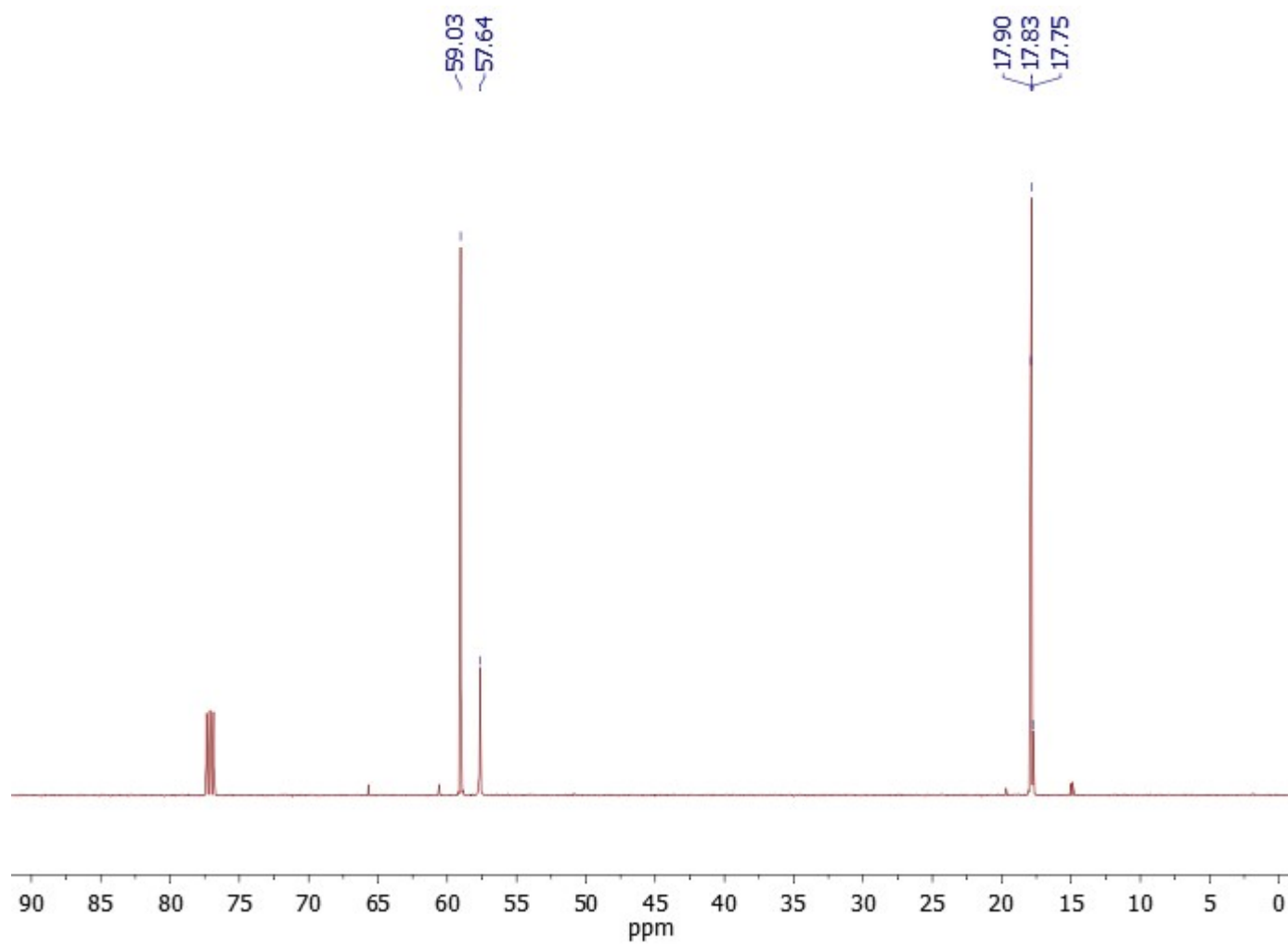


Figure S27 ^{13}C NMR spectrum for synthesis with ethanol

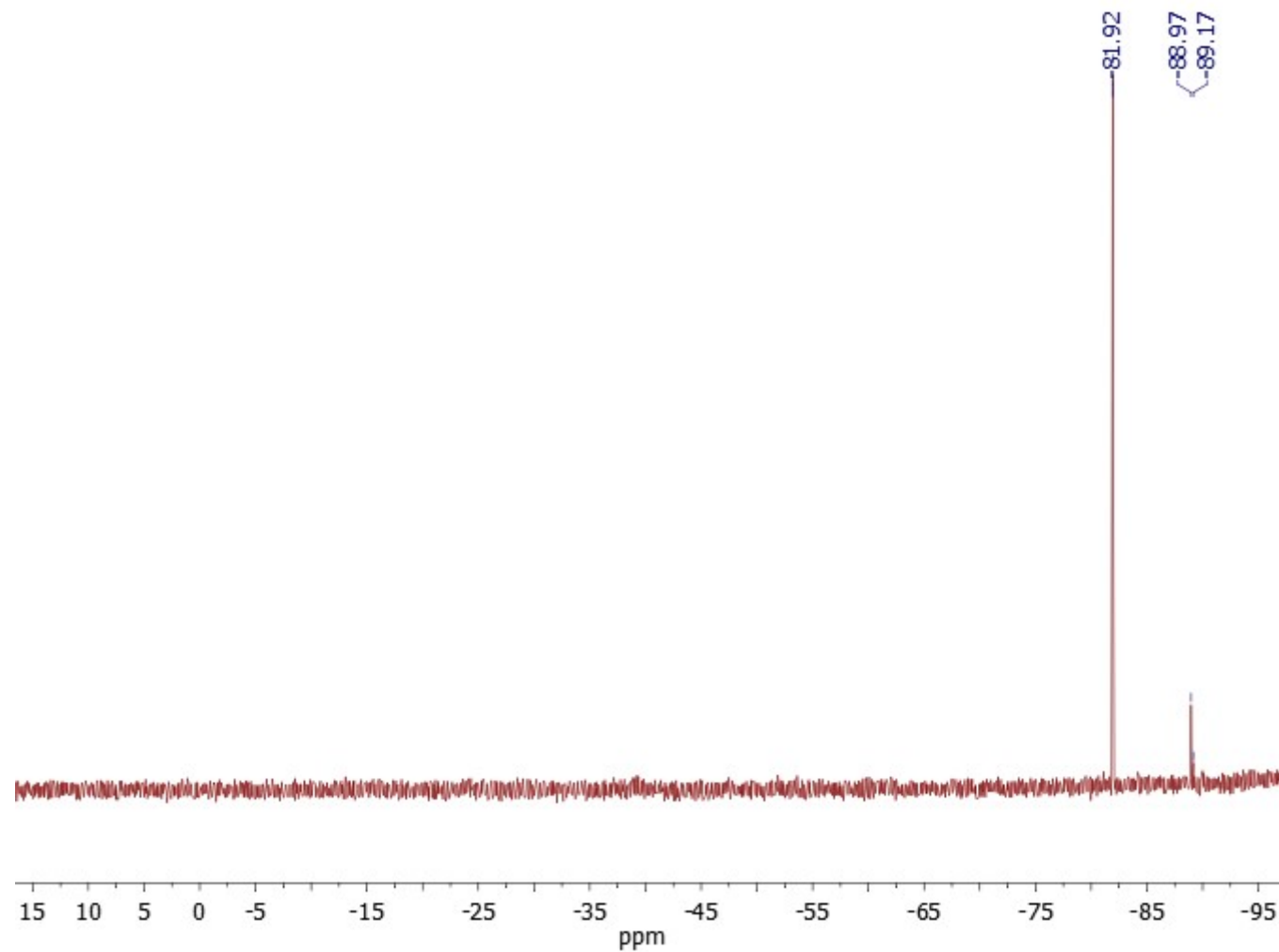


Figure S28 ^{29}Si NMR spectrum for synthesis with ethanol

NMR for tetrabutoxysilane synthesis

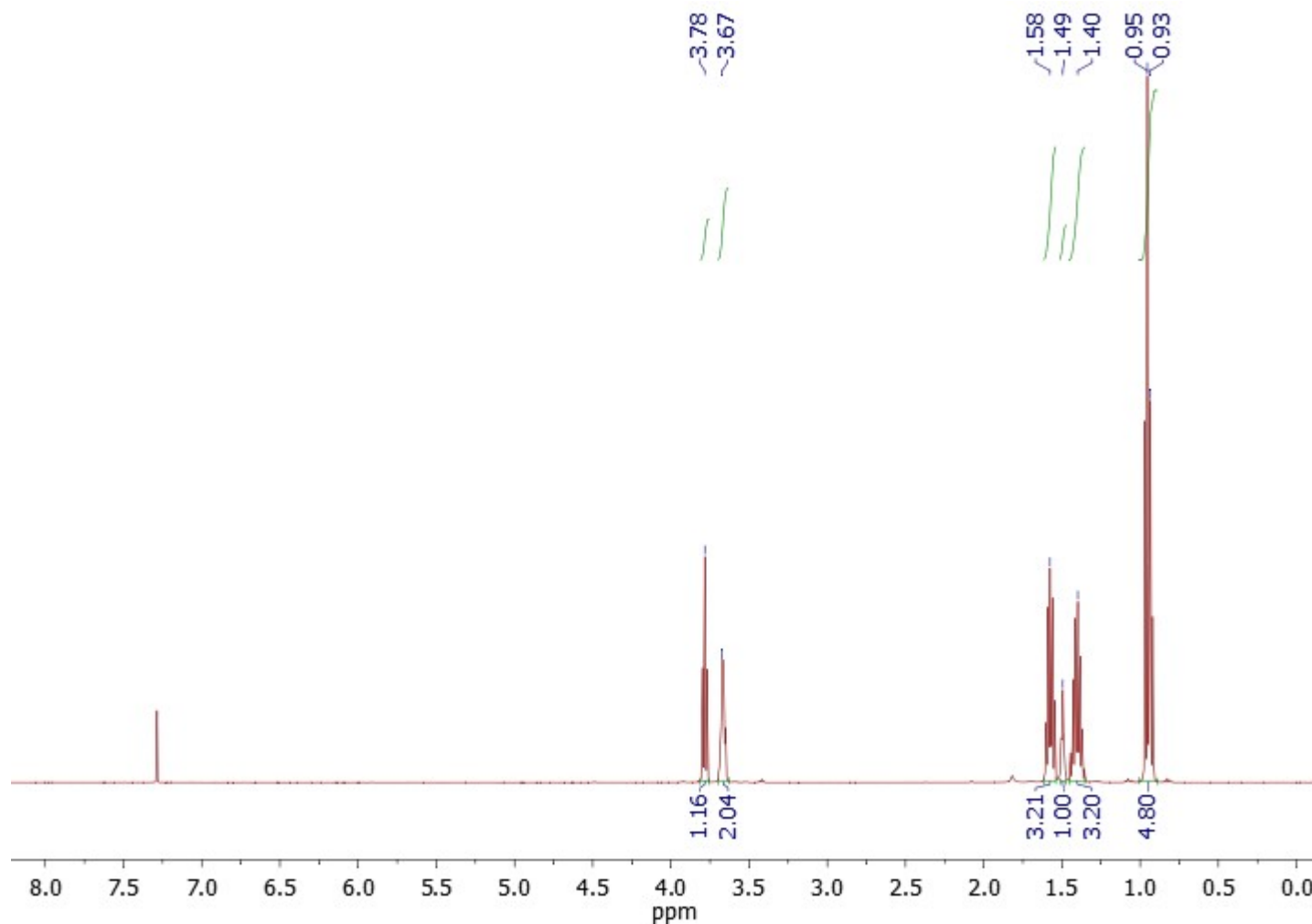


Figure S29 ¹H NMR spectrum for synthesis with butanol

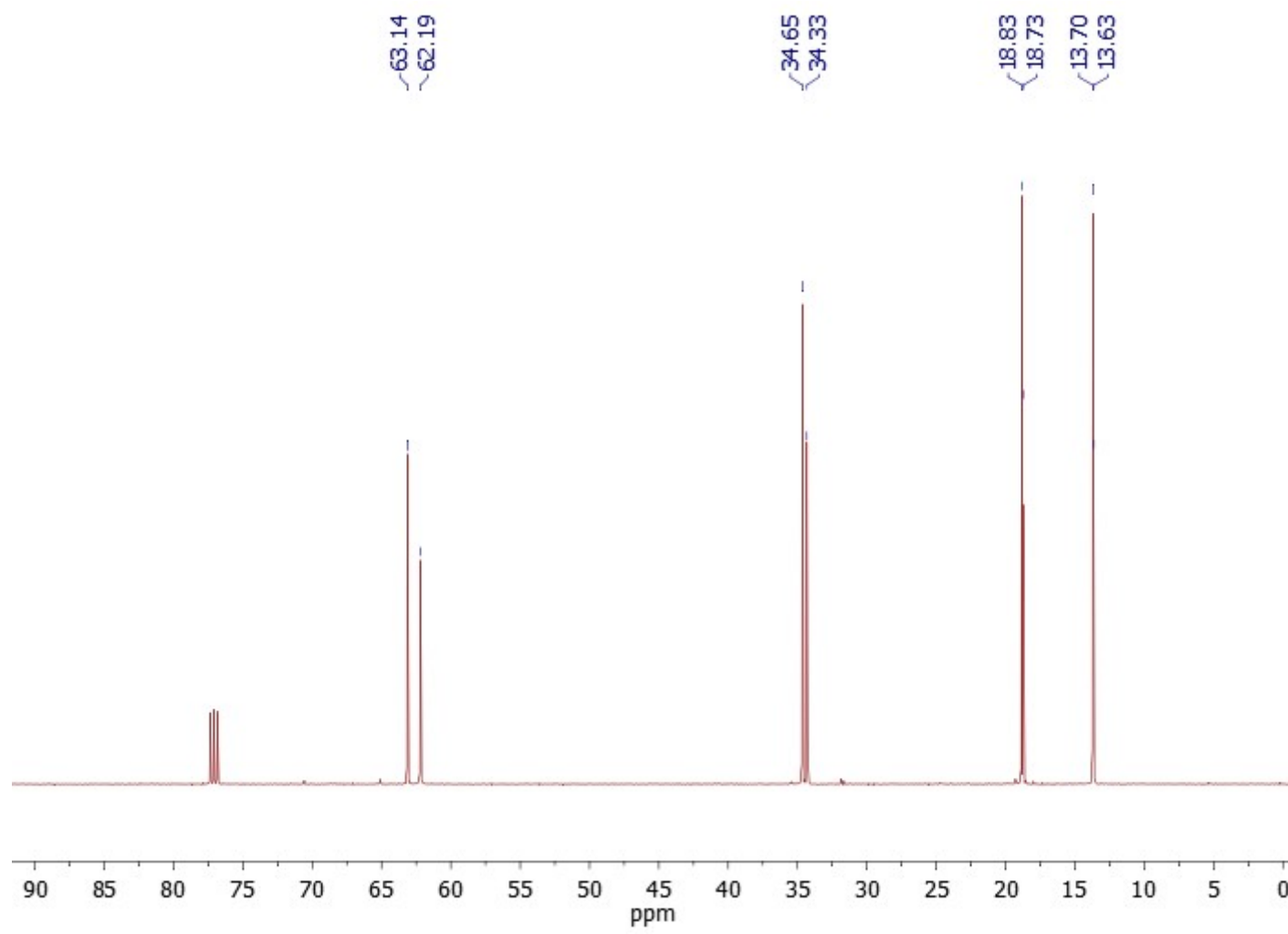


Figure S30 ^{13}C NMR spectrum for synthesis with butanol

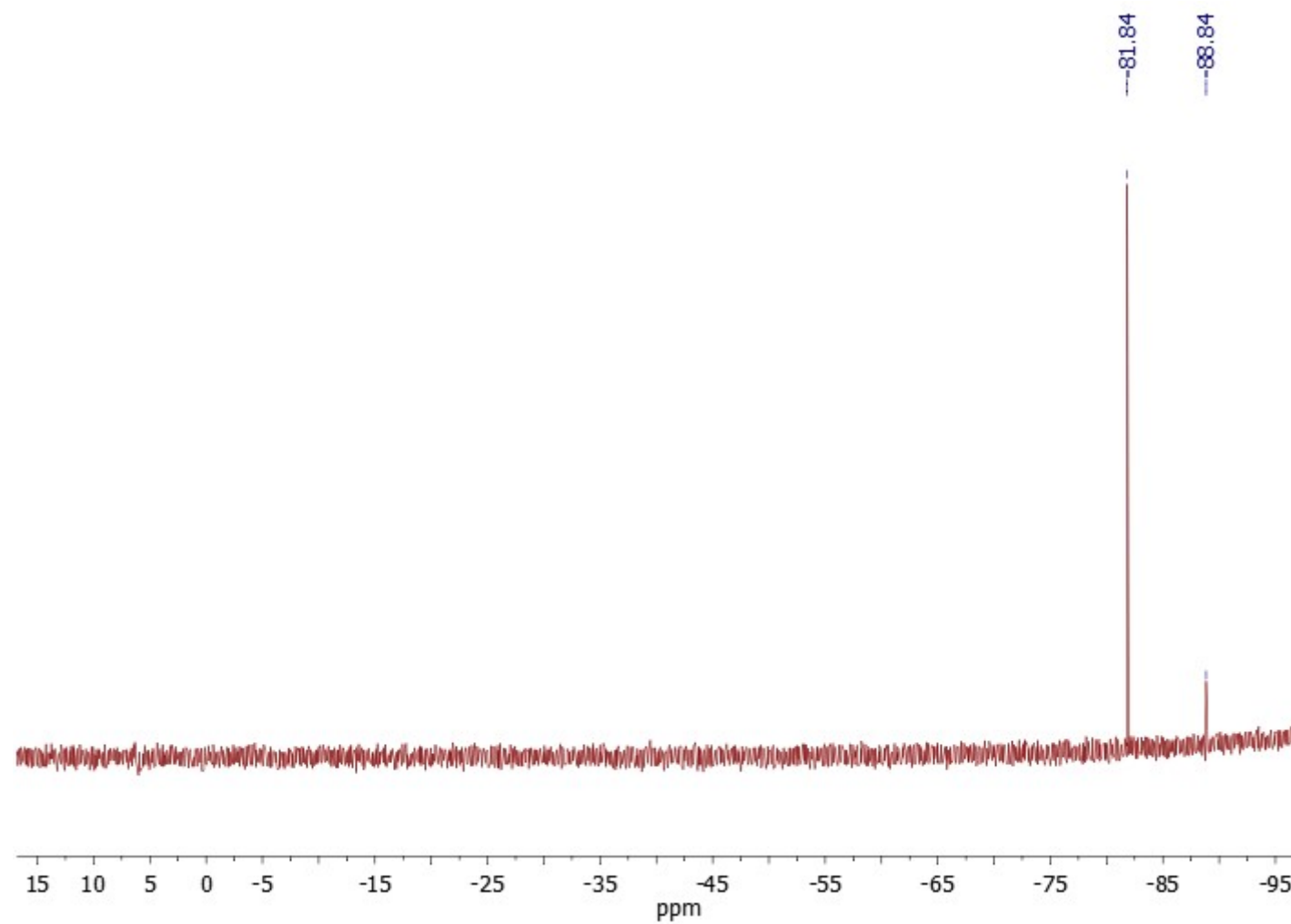


Figure S31 ^{29}Si NMR spectrum for synthesis with butanol

NMR for tetra(2-ethoxy)ethoxysilane synthesis

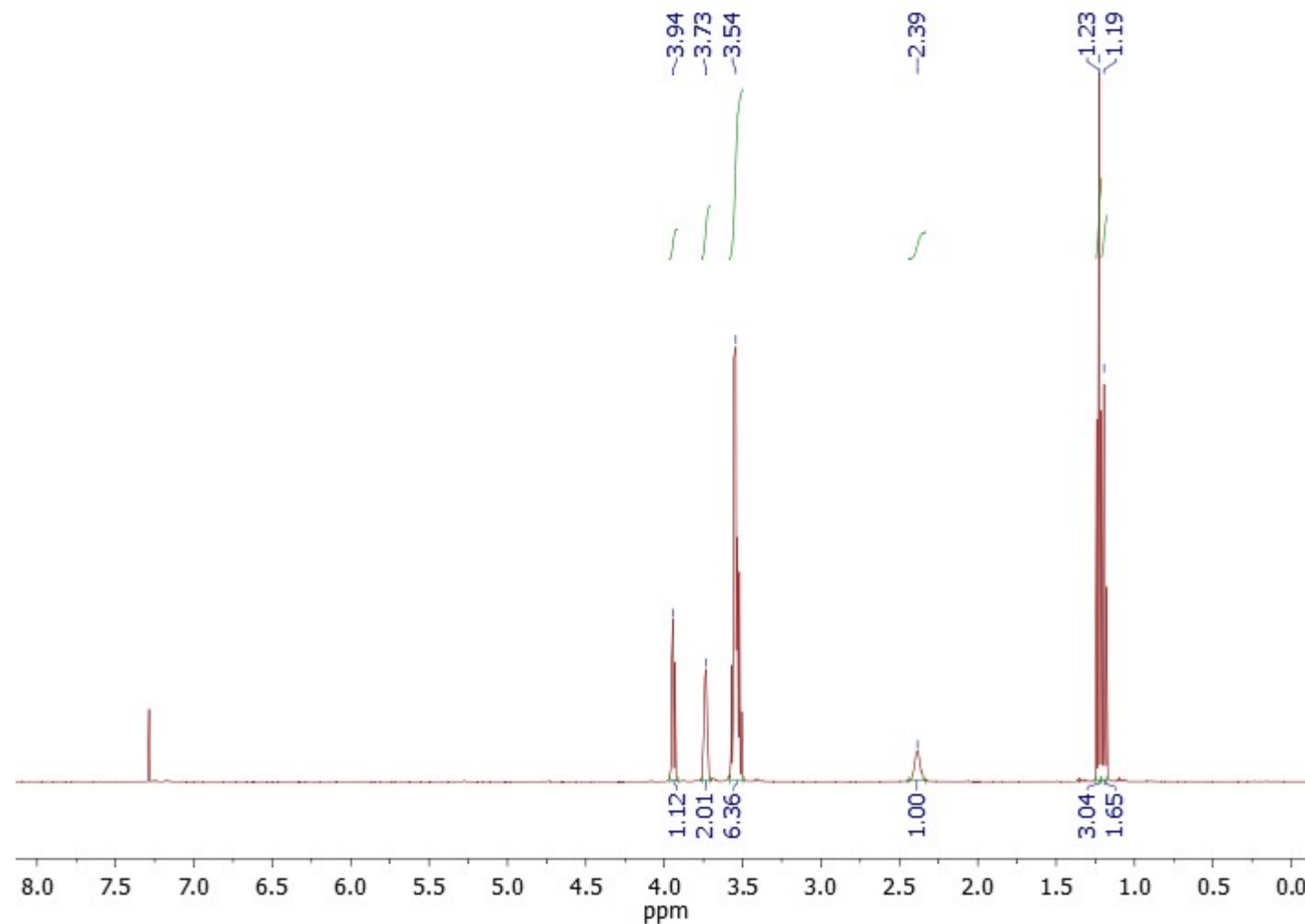


Figure S32 ¹H NMR spectrum for synthesis with ethoxyethanol

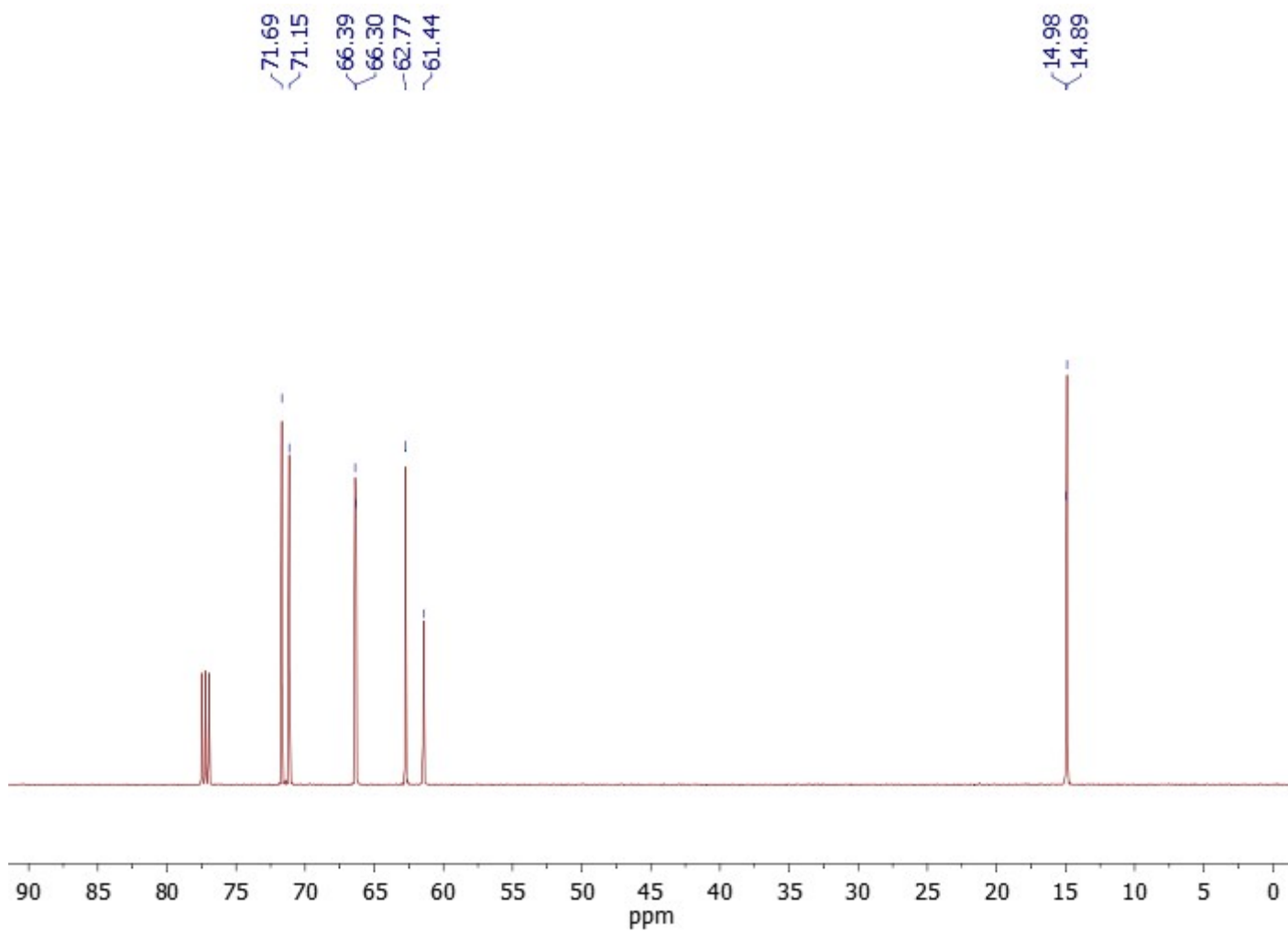


Figure S33 ^{13}C NMR spectrum for synthesis with ethoxyethanol

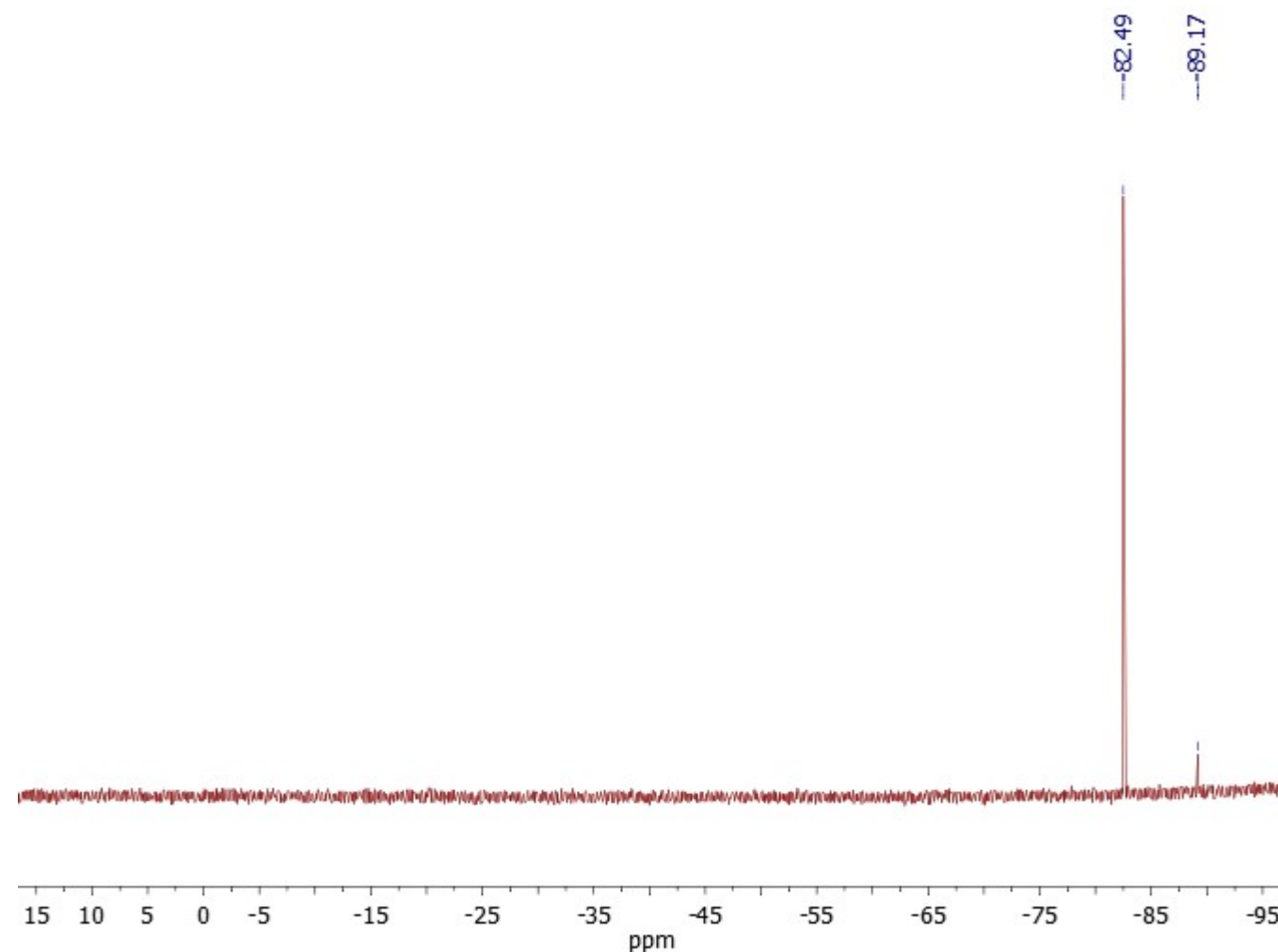


Figure S34 ^{29}Si NMR spectrum for synthesis with ethoxyethanol

4.3. PXRD – date

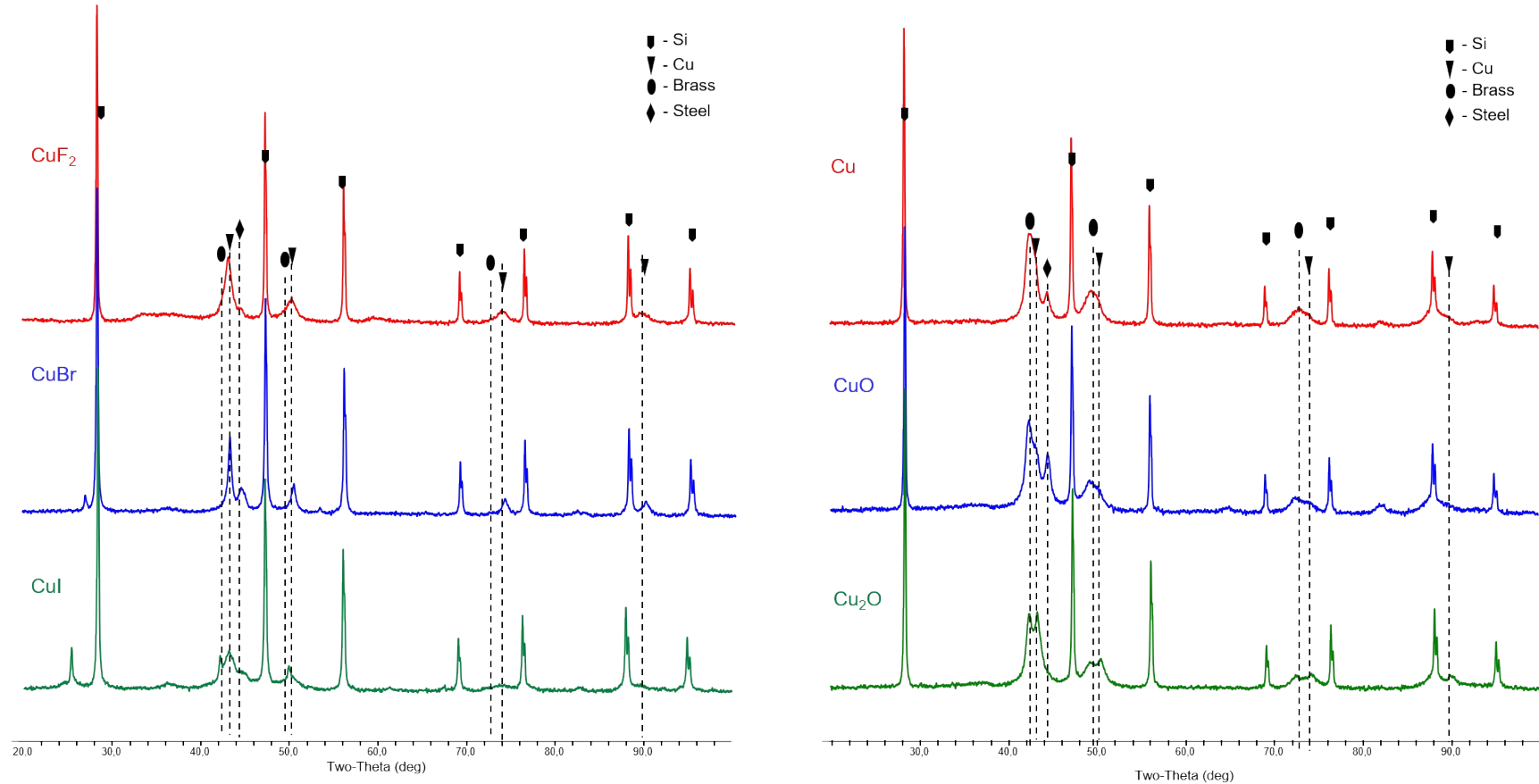


Figure S35 PXRD data of contact mass samples after reaction $\text{Si} + \text{MeOH}$ (20% CuCl), acceleration 19 g, $T = 100^\circ\text{C}$, 300 min.

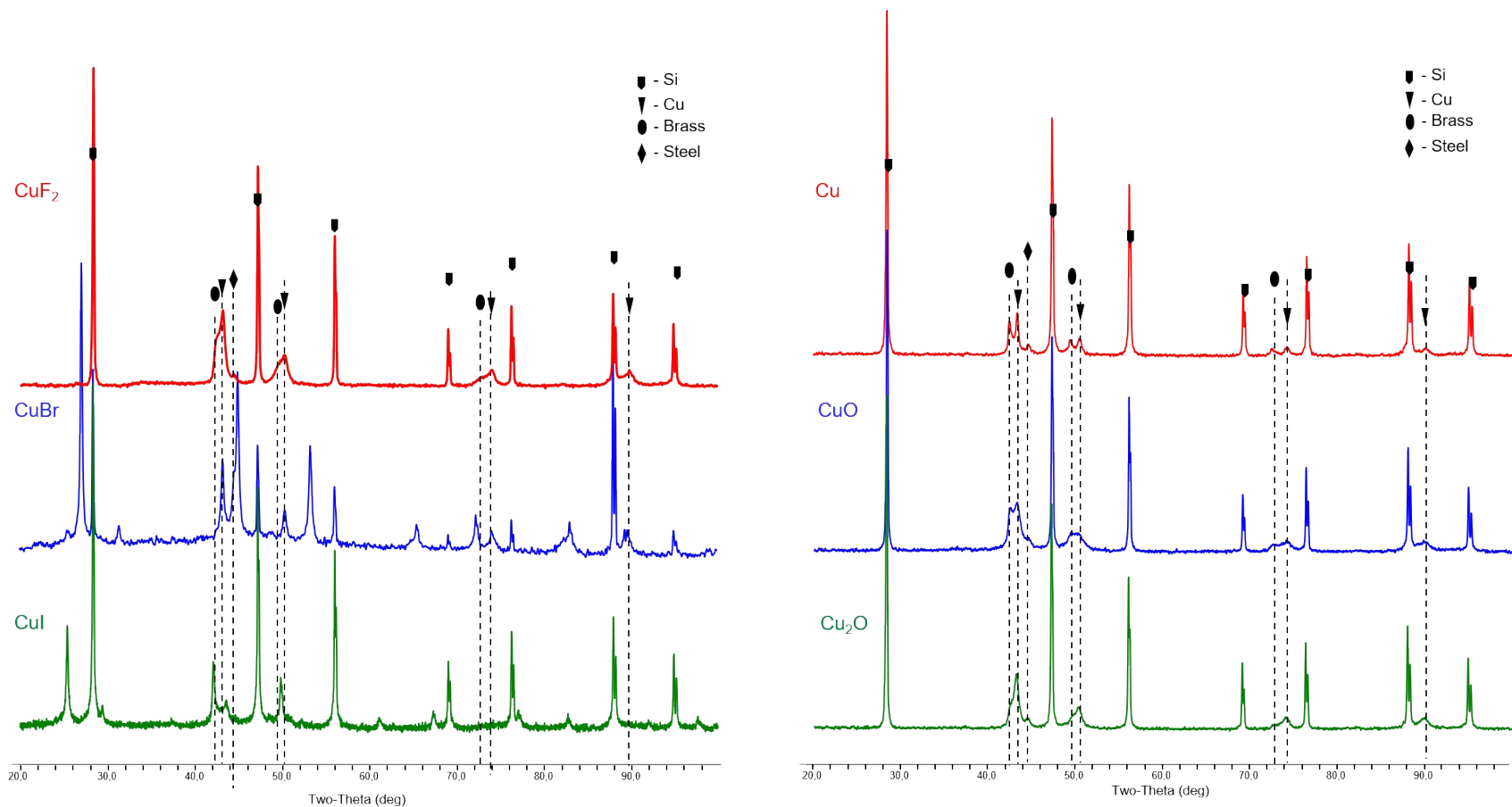


Figure S36 PXRD data of contact mass samples after reaction Si + MeOH (20% w Cu_nX_m), acceleration 19 g, T = 250 °C, 30 min.

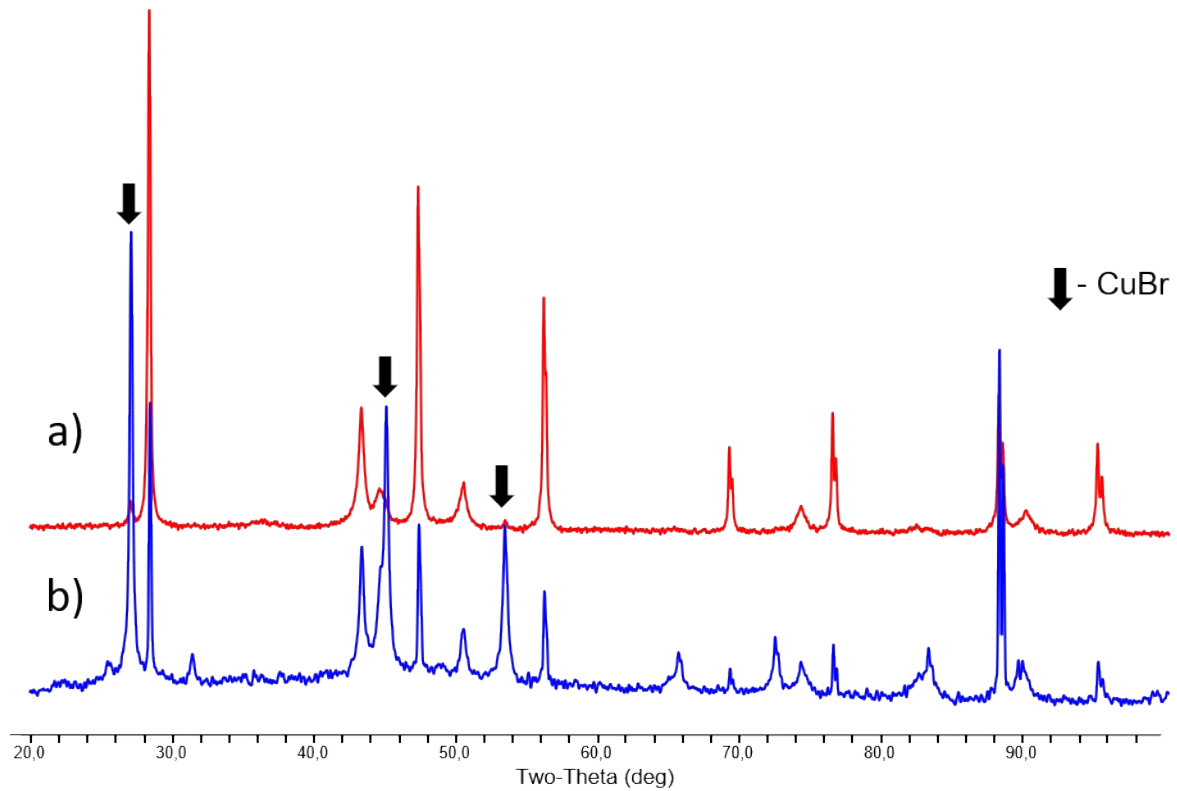


Figure S37 PXRD data of contact mass samples after reaction Si + MeOH (20% w CuBr), acceleration 19 g, a) T = 100 °C, 300 min. b) T = 250 °C, 30 min.

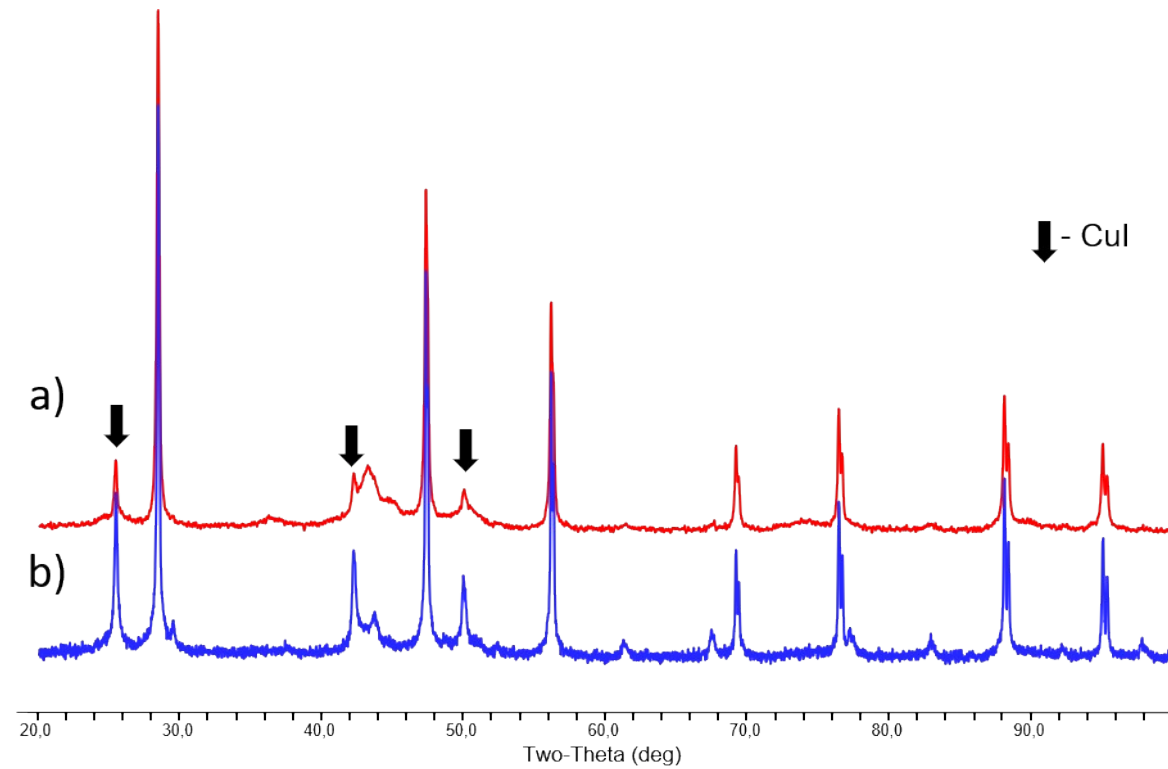


Figure S38 PXRD data of contact mass samples after reaction Si + MeOH (20% w CuI), acceleration 19 g, a) T = 100 °C, 300 min. b)
T = 250 °C, 30 min.

4.4. GLC-MS – spectra

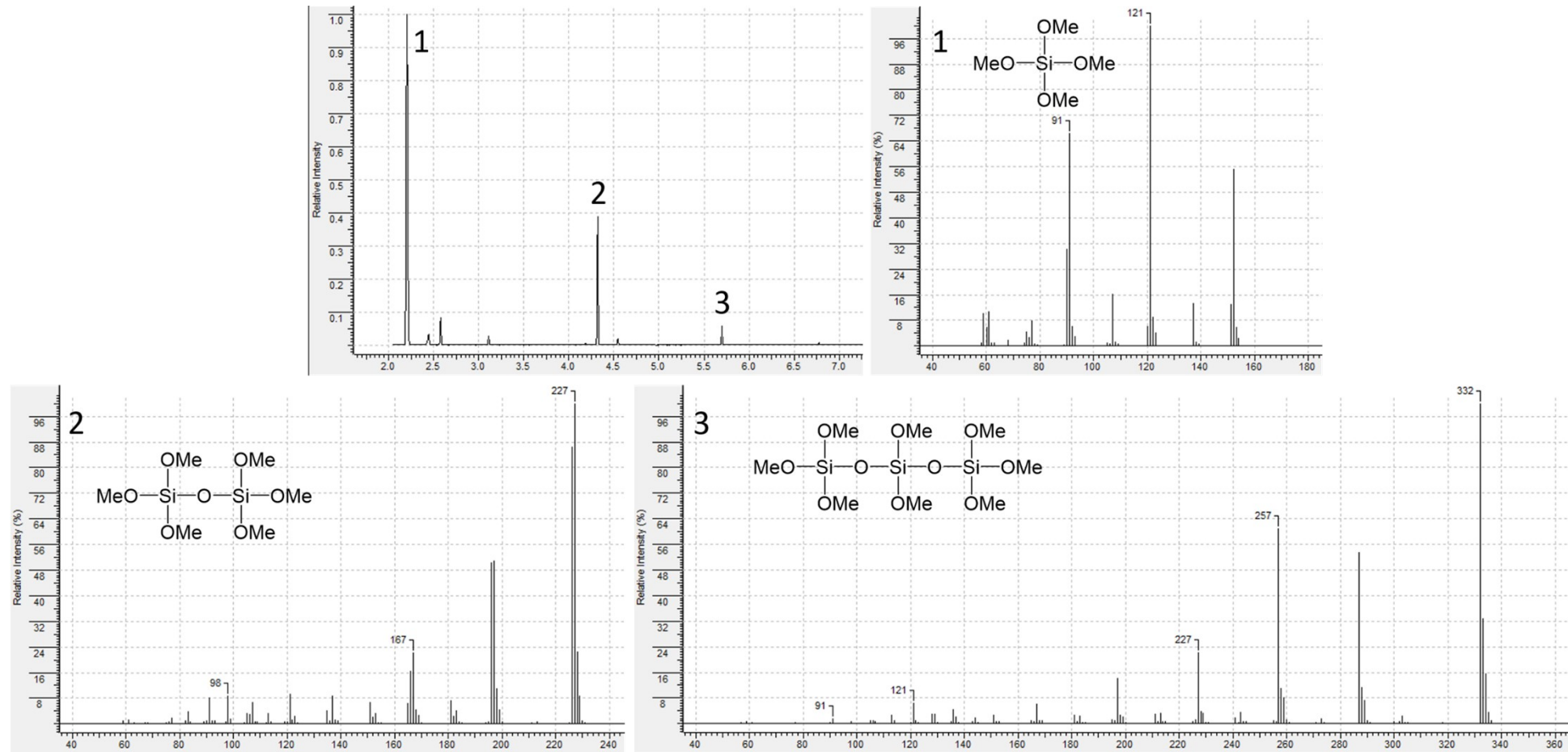


Figure S39 GLC-MS – spectra of products mixture after the synthesis with methanol

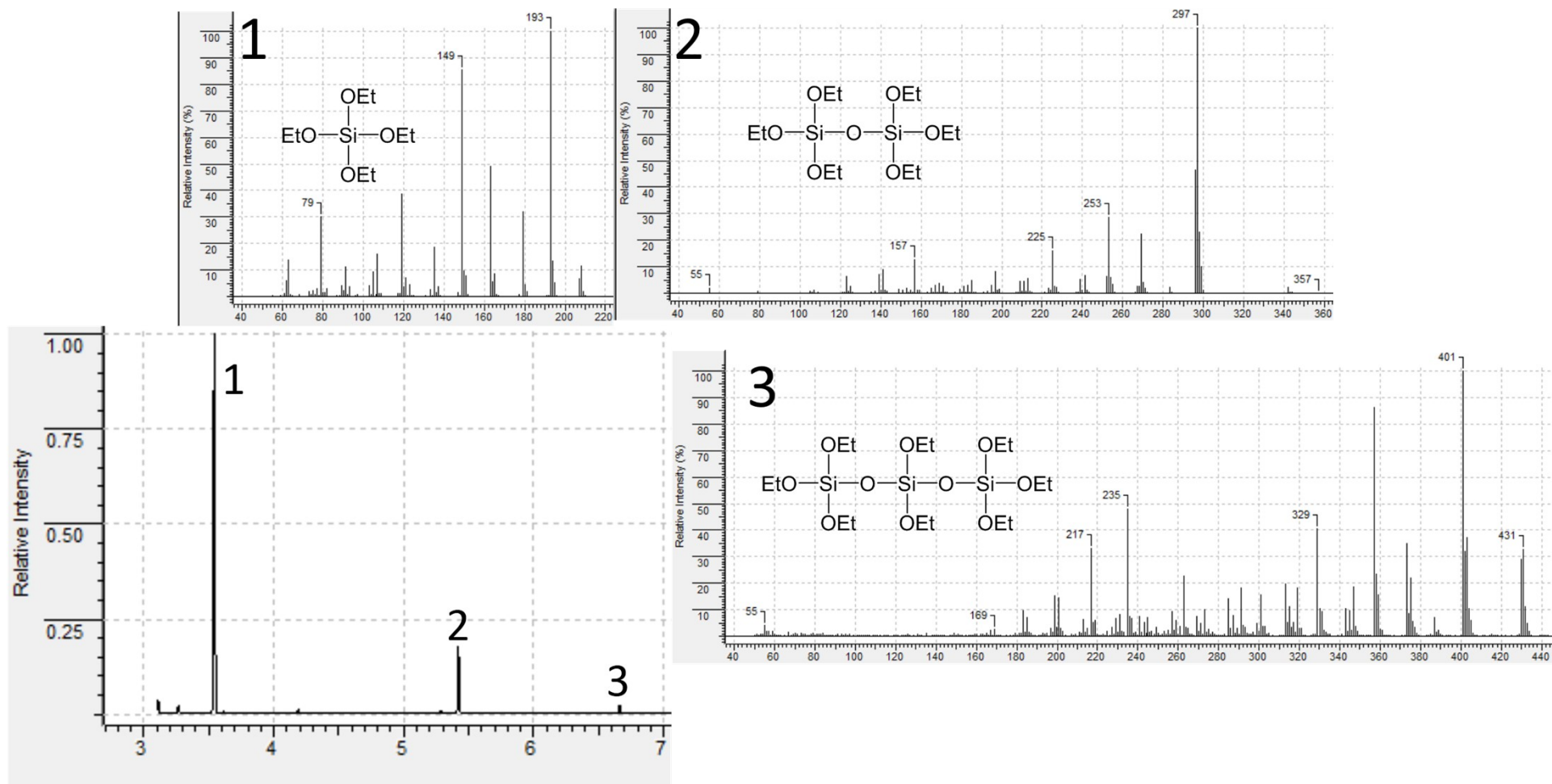


Figure S40 GLC-MS – spectra of products mixture after the synthesis with ethanol

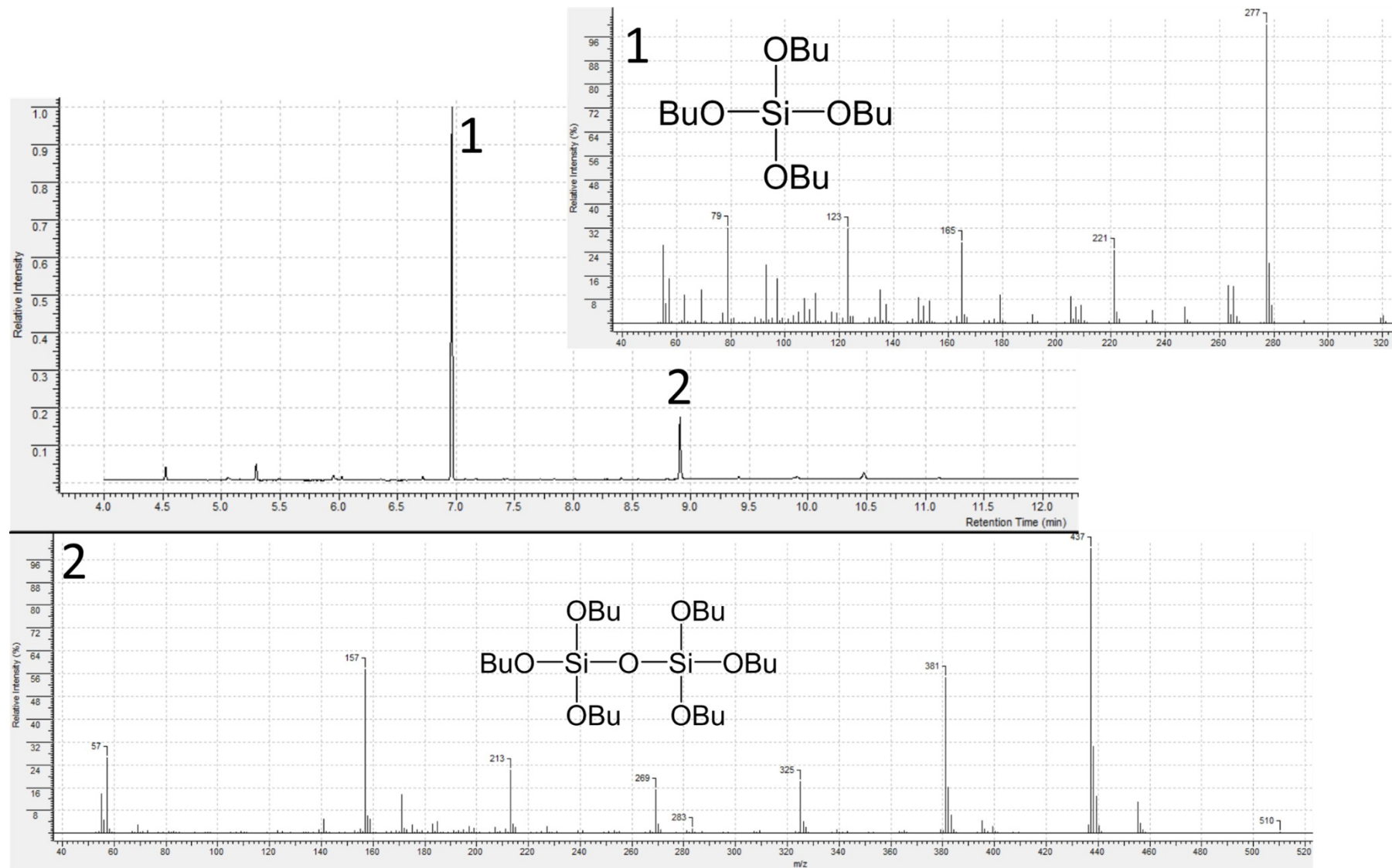


Figure S41 GLC-MS – spectra of products mixture after the synthesis with butanol

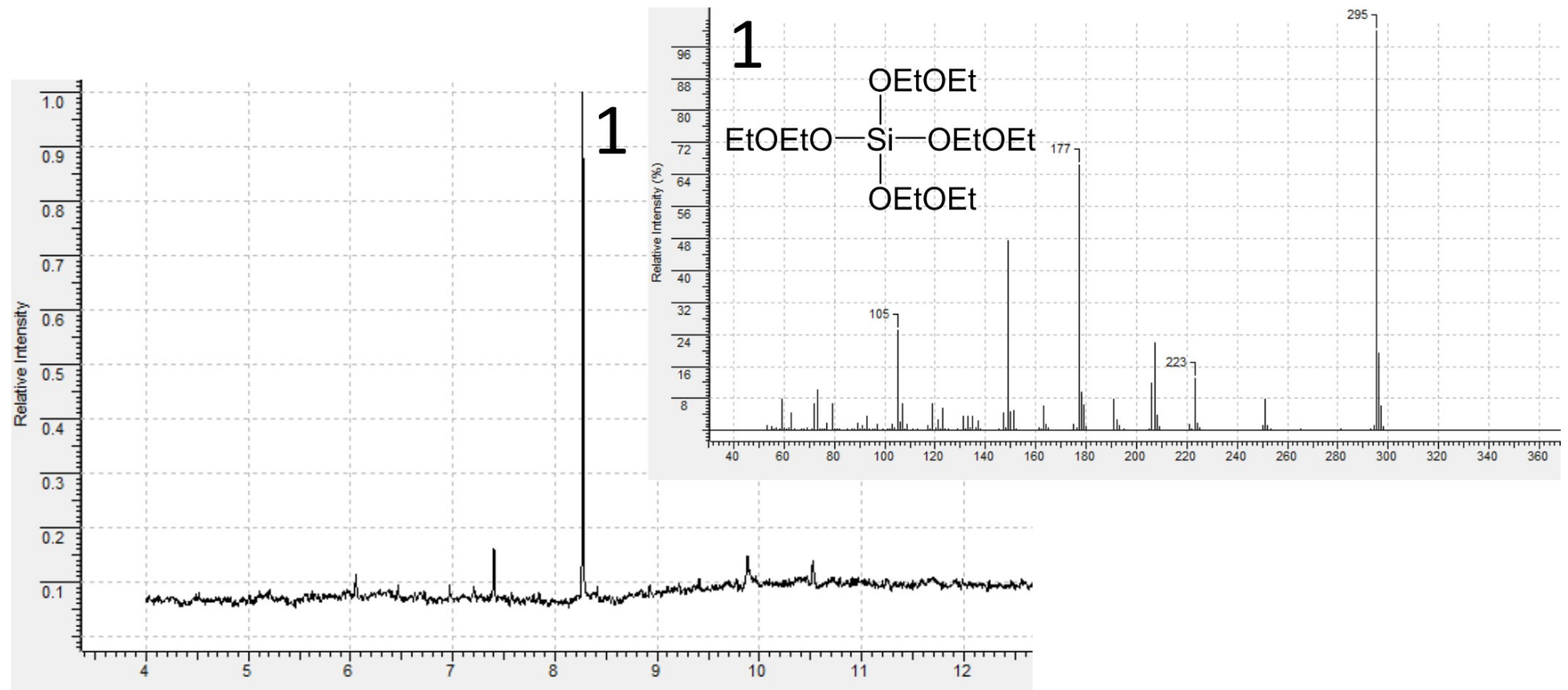


Figure S42 GLC-MS – spectra of products mixture after the synthesis with ethoxyethanol

4.5. XPS – spectra

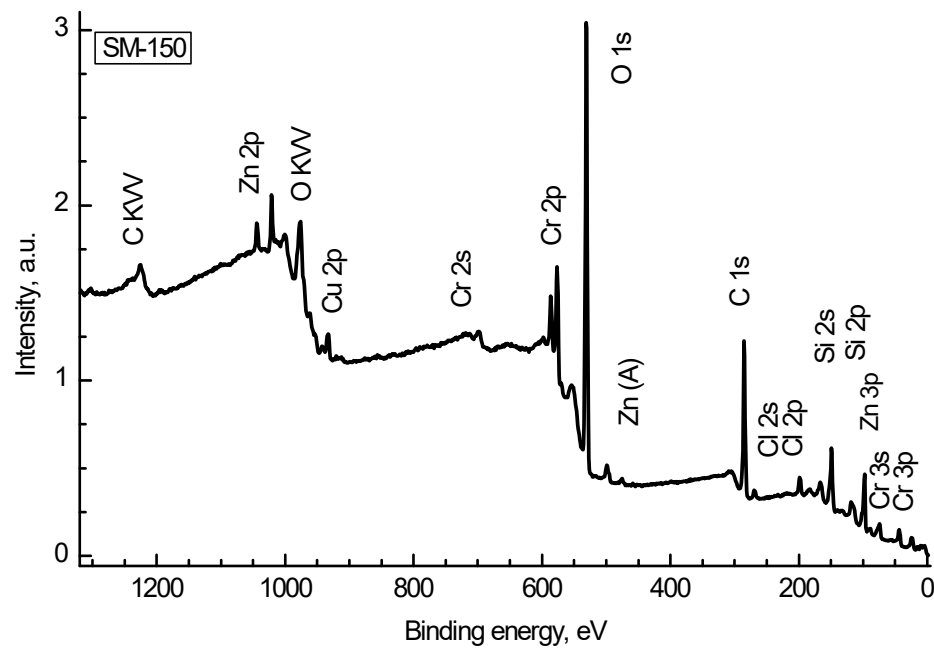


Figure S43. Survey spectrum of sample SM-150.

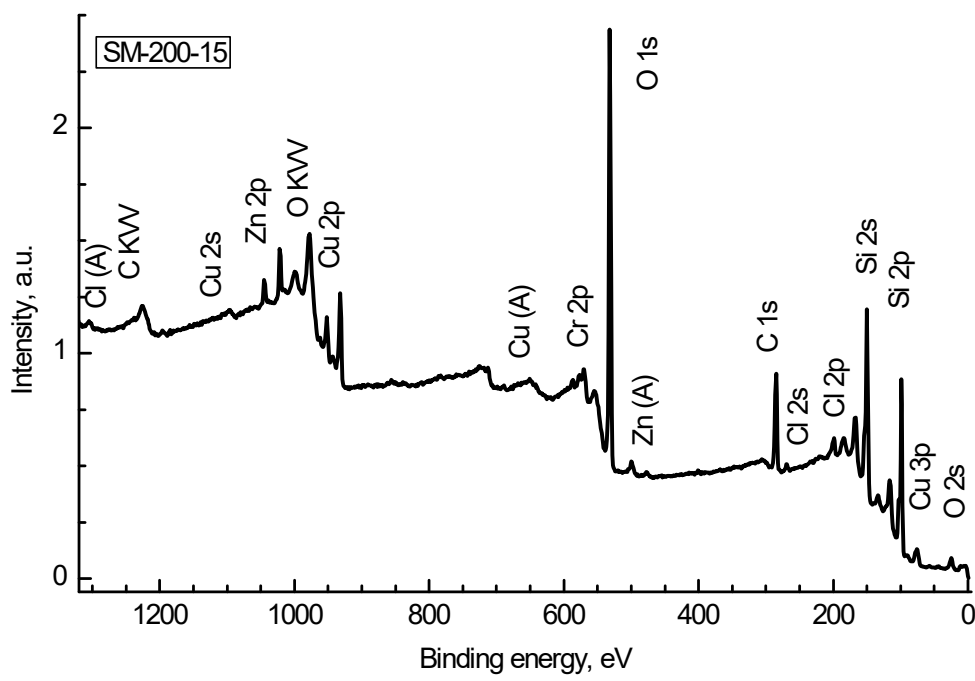


Figure S44. Survey spectrum of sample SM-200-15.

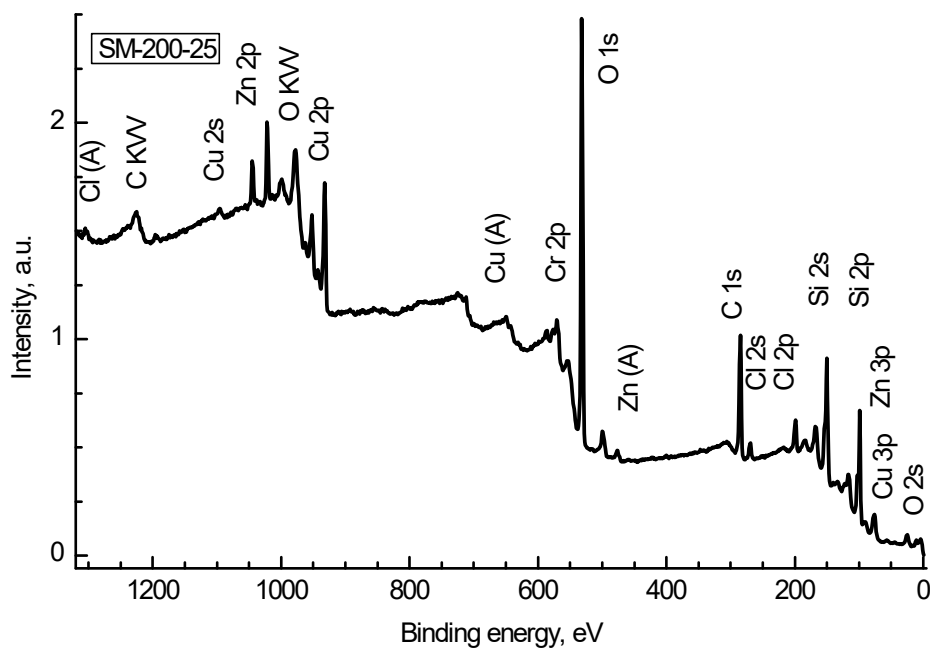


Figure S45 Survey spectrum of sample SM-200-25.

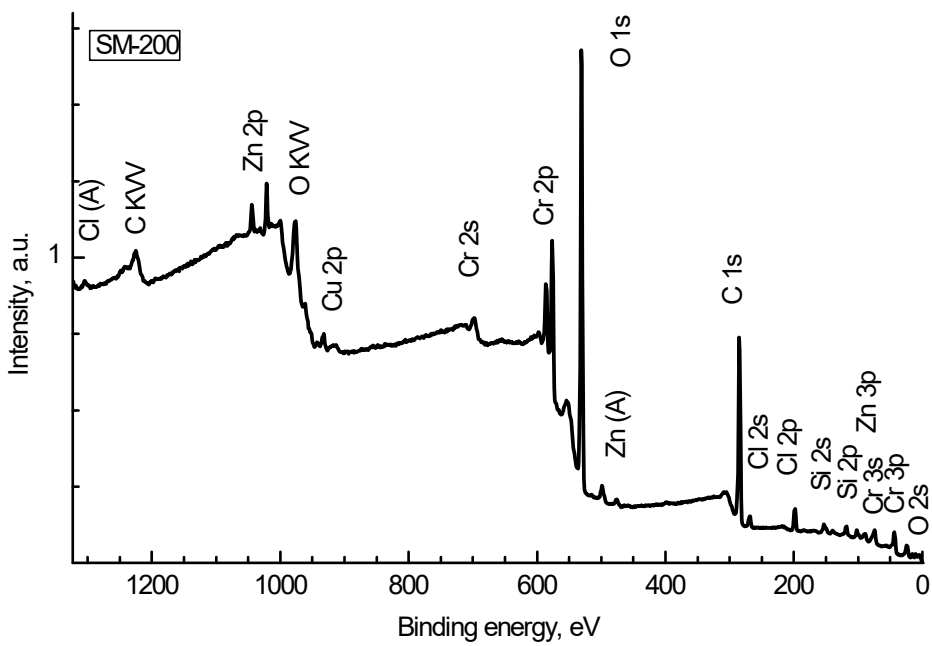


Figure S46 Survey spectrum of sample SM-200.

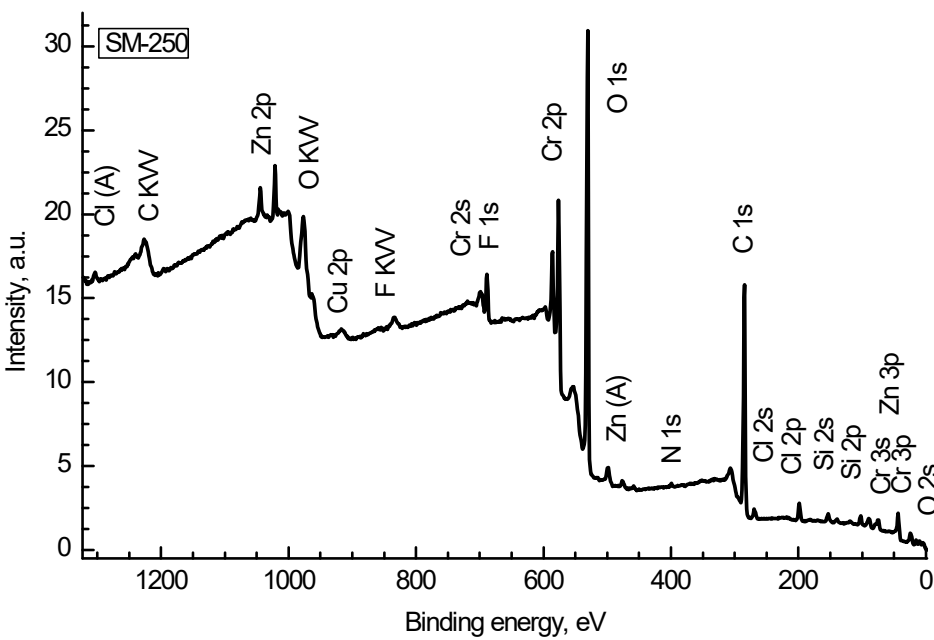


Figure S47 Survey spectrum of sample SM-250.

Figure S48 shows the Si 2p photoelectron spectra of the studied samples, normalized to the intensity of the high-energy peak corresponding to the Si⁴⁺ state, and qualitatively reflecting the relative concentrations of the Si⁴⁺ and Si⁰ states.

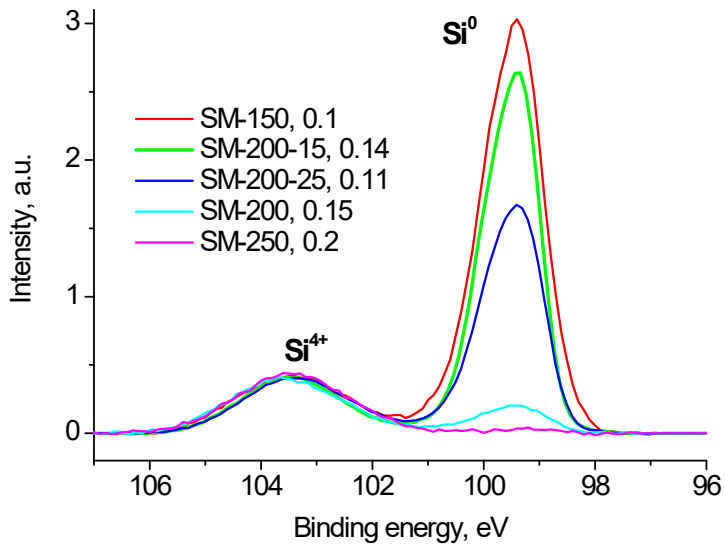


Figure S48 Photoelectron spectra of Si 2p of the studied samples, the spectra are normalized to the intensity of the high-energy peak.

For quantitative estimates, the spectra were decomposed into components. The low-energy part of the spectrum is described by the $\text{Si } 2\text{p}_{3/2}-2\text{p}_{1/2}$ spin-orbital doublet with a splitting of 0.61 eV and a characteristic ratio of 2/1 (Figure S49). Due to the low signal-to-noise ratio in the region of binding energies of about 99.3 eV in the case of the spectra of sample SM-250, the surface charging was taken into account by the peak of the Si^{4+} state, to which the binding energy of 103.44 eV was assigned, and the values of the binding energies for the Si^0 state given in Table S4 are approximate.

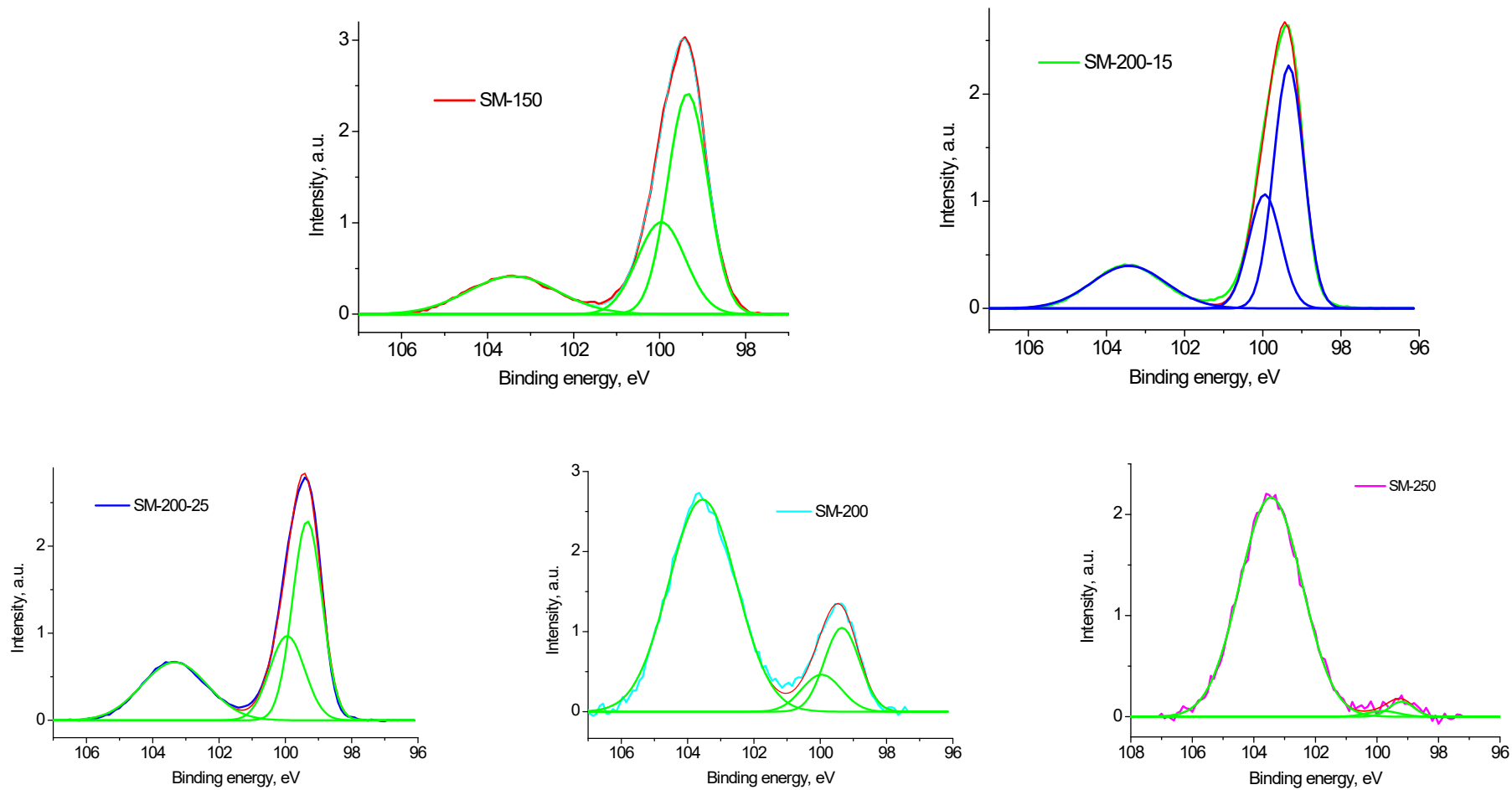


Figure S49 Si 2p photoelectron spectra of the studied samples; fitting with some Gaussian profiles.

Taking into account the possibility of copper reduction under the action of X-ray radiation, the Cu 2p spectra were recorded at the beginning and at the end of the experiment (Figure S50). To reduce the degree of influence, the registration of the spectra was begun with the Cu 2p spectrum.

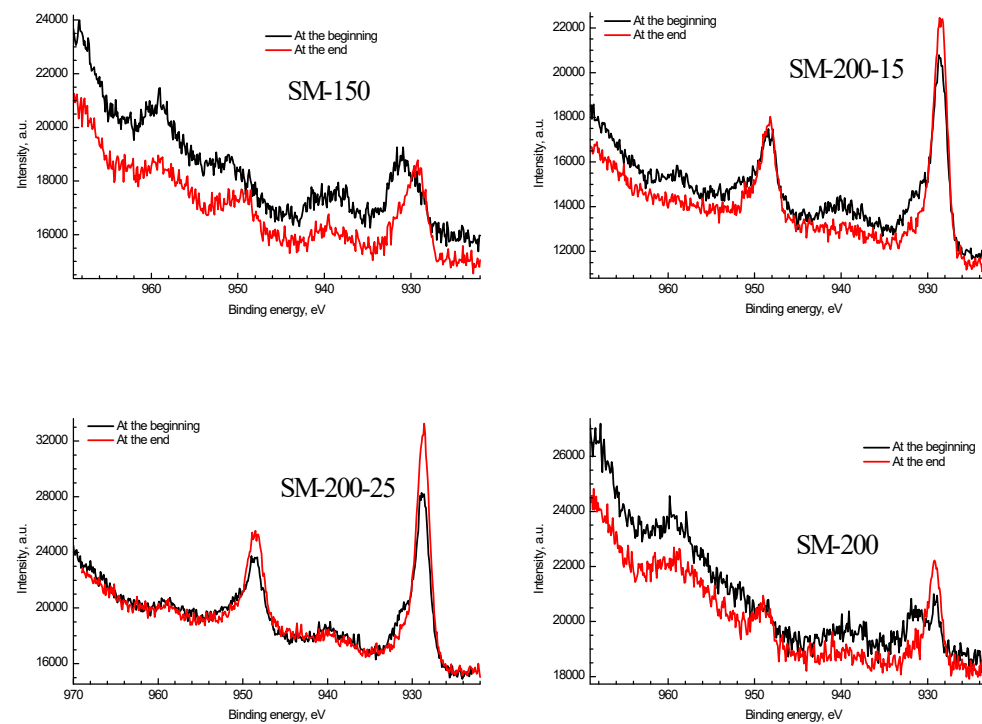


Figure S50 Effect of X-ray radiation on the chemical state of copper atoms.

Figure S50 clearly demonstrates the increase in the intensity of the low-energy peak at the end of the photoelectron spectra acquisition. Therefore, the fraction of the Cu²⁺ state determined from the considered spectra can be higher. Since the Cu 2p_{1/2} spectrum partially overlaps with the Co LMM Auger spectrum, further analysis was carried out only for the Cu 2p_{3/2} spectrum. Figure S51 shows that the spectrum of sample SM-150 stands out noticeably, which is due to the large fraction of the Cu²⁺ state in the sample, as indicated by intense satellites at ~944 eV, an intense signal at ~ 936 eV, and a shift of the main peak to the region of high binding energies relative to peaks of other samples. To determine the relative fractions of different chemical states, approximations of the Cu 2p spectra with some components (Figure S52), based on the characteristics of the peaks given in [11] were used. The results are shown in Table S5.

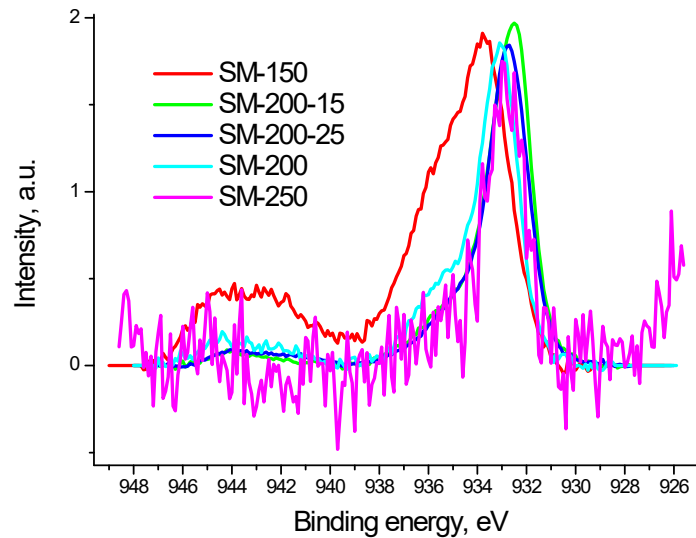


Figure S51 The Cu 2p_{3/2} photoelectron spectra of the studied samples.

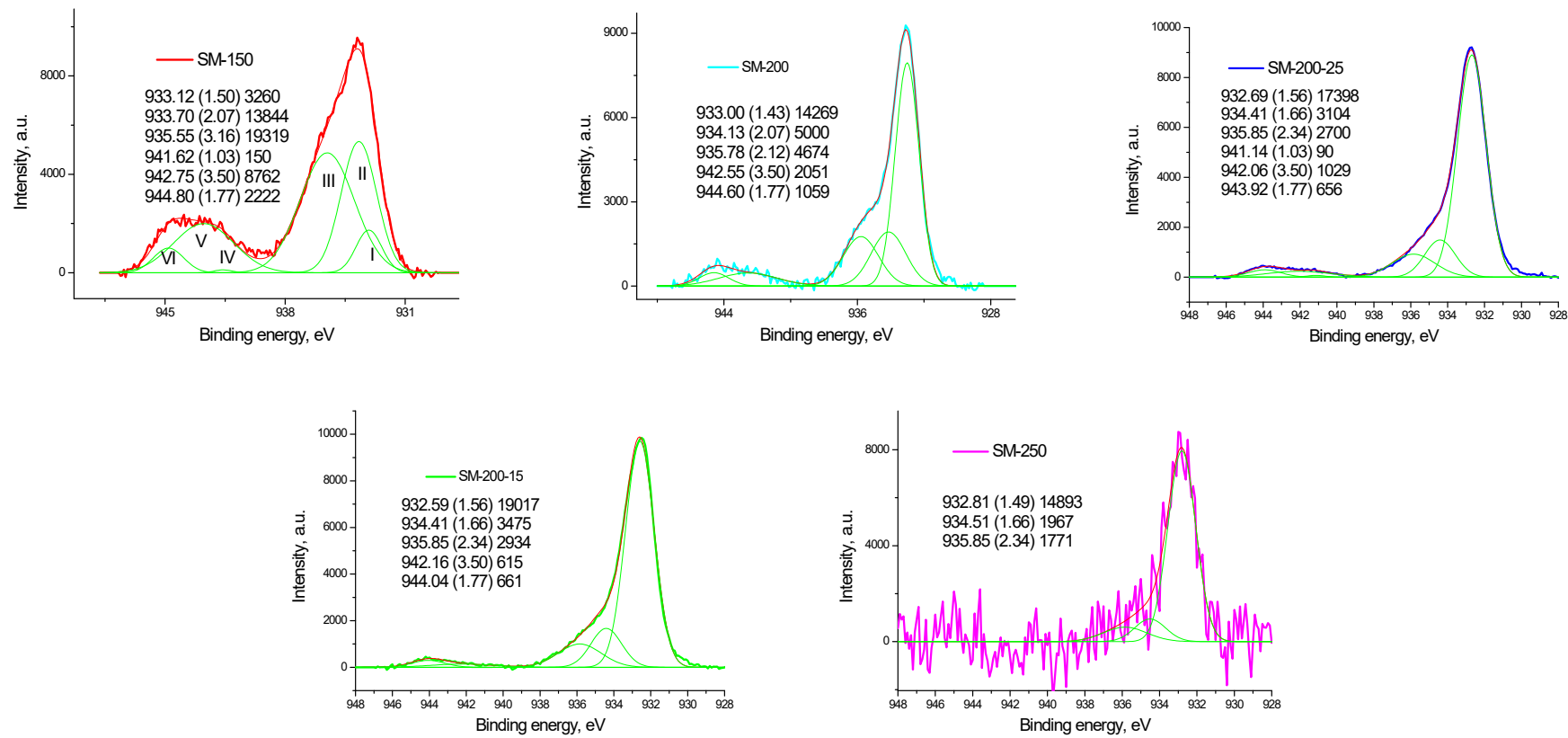


Figure S52 The Cu 2p_{3/2} photoelectron spectra of the studied samples approximated with some components.

From the data given in Table S5, it follows that the fractions of the Cu²⁺ state in samples SM-150, SM-200-15, SM-200-25, SM-200 and SM-250 are 0.93, 0.29, 0.30, 0.47 and 0.20, respectively.

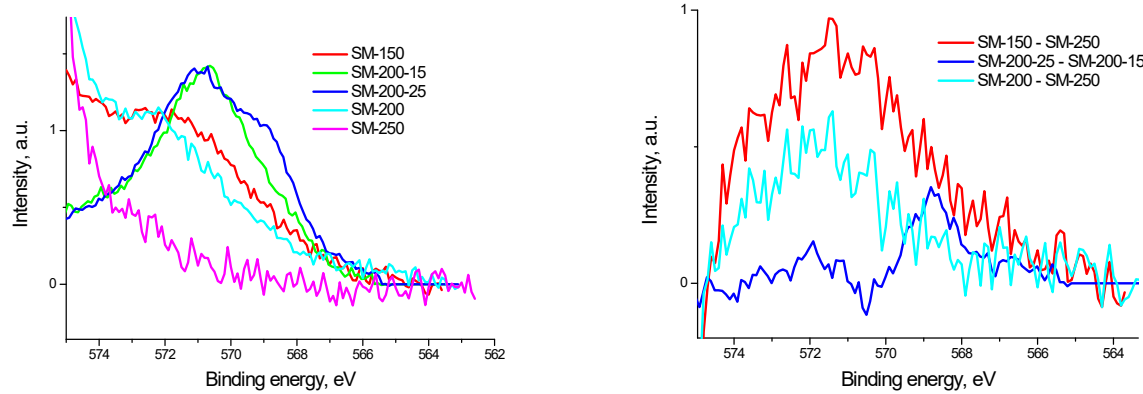


Figure S53 Region of the $\text{L}_3\text{M}_{4,5}\text{M}_{4,5}$ Auger spectra of the studied samples and their difference spectra.

Figure S53 shows the $\text{L}_3\text{M}_{4,5}\text{M}_{4,5}$ Auger spectra of the studied samples, partially overlapping with the Cr $2\text{p}_{3/2}$ spectra and some difference spectra for which the Auger peak energies were determined and presented in Table S6. Due to the highest Cu concentration in sample SM-200-25, the corresponding Auger spectrum has the best signal-to-noise ratio. There are clearly two peaks in the spectrum; subtraction of the spectrum of sample SM-200-15 was used to determine the position of the low-energy peak. The binding energies of these peaks are 571.1 and 568.8 eV, and the corresponding kinetic energies and Auger parameters are given in Table S6. The Auger parameter of 1848.3 eV, according to the data presented in Table S6, occupies an intermediate position between the values characteristic of CuCl (~1847.4 eV) and Cu_2O (1849.17-1849.5 eV). Similarly, the Auger parameter of 1850.65 eV can be assigned to both Cu_2O and Cu^0 . In this case, we do not consider the close values of the Auger parameters related to the state of Cu^{2+} due to the absence of their characteristic satellites in the region of binding energies of about 942 eV with an intensity approximately equal to half the intensity of the main peak. However, taking into account the binding energy of the low-energy peak at 932.8 eV and

the size effect [12, 13], which is more pronounced in the Auger spectrum, the Auger peak with a binding energy of 568.75 eV should be attributed to the Cu⁰ state [13].

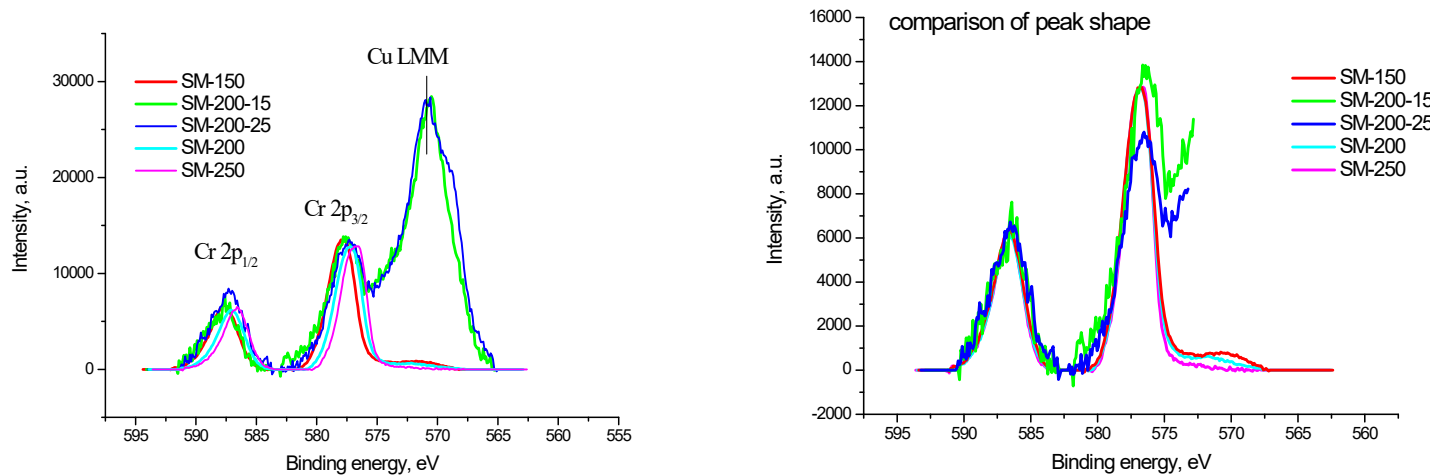


Figure S54 Photoelectron spectra of Cr 2p and Cu LMM Auger spectra of the studied samples.

Figure S54 shows that the Cr 2p photoelectron spectra and Cu LMM Auger spectra overlap in the case of samples SM-200-15 and SM-200-25 at large ratios of Cu and Cr concentrations. If the positions of the main Cu LMM Auger peaks are the same, then that of the Cr 2p peaks are noticeably different, which, apparently, indicates the manifestation of differential charging, since the Cr 2p line shapes when they are combined in the case of samples SM-200, SM-150, and SM-250 are virtually indistinguishable. The Cr 2p_{1/2} peaks of samples SM-200-15 and SM-200-25 are characterized by a slight broadening, which is caused by a significantly lower chromium concentration and, accordingly, a greater inhomogeneity of the samples, which manifests itself in a decrease in the signal-to-noise ratio. As for the Cr 2p_{3/2} peaks, their shape is significantly affected by the overlap with the Cu LMM

Auger spectrum and the features of background subtraction. Table S7 shows the characteristics of the Cr 2p photoelectron spectra. The table shows the dependence of the $2p_{1/2}$ - $2p_{3/2}$ spin-orbit splitting on the Cu/Cr ratio. It should be noted that for pure chromium, the spin-orbit splitting is 9.2 eV [12].

In other words, the higher the chromium concentration in the sample, the closer the spin-orbit splitting to the reference value for Cr_2O_3 . It was shown that with an increase in the oxidation state of Cr atoms, the spin – orbit splitting also increases [14]. At the same time, it decreases with an increase in 3d electrons and for Cr^{6+} is in the range of 8.7-9.4 eV [15]. Thus, the values of 10 and 10.2 eV should be attributed to the influence of the nearest environment on the relative components of the multiplet splitting in the Cr 2p spectra, which manifests itself at low Cr concentrations in the samples.

Figure S55 shows the C 1s spectra of the studied samples, from which it can be seen that the positions of the main peaks are very different. It should be noted that the surface charging was taken into account according to the state of Si^0 , which is distinguished in the corresponding Si 2p peaks. As a rule, in the C 1s spectra, the peak with the highest intensity is attributed to the C–C/C–H state, the binding energy of which is in the range 284.6 - 285.2 eV. However, in most cases it is believed that the binding energy of this state is in the range of 284.8-285.0 eV. The spectra of samples SM-200-15 and SM-200-25 have almost identical shapes with close binding energies of the main peaks: 285.4 and 285.2 eV, which should be attributed to the C-C/C-H state and, in turn, indicate the presence of differential charging. Figure S56 shows the selection of various states in these spectra, which, due to differential charging, may be assigned to the C-C/C-H, C-OH/C-O-C and C(O)O groups.

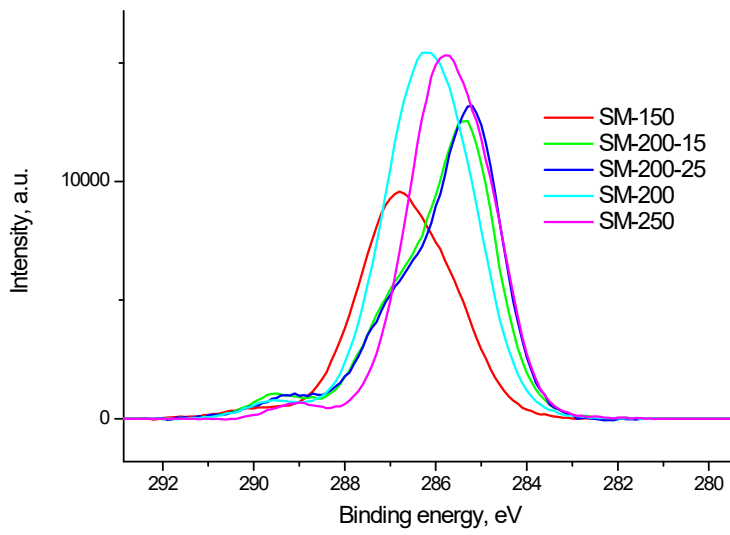


Figure S55 The C 1s photoelectron spectrum of samples SM-150, SM-200-15, SM-200-25, SM-200, SM-250.

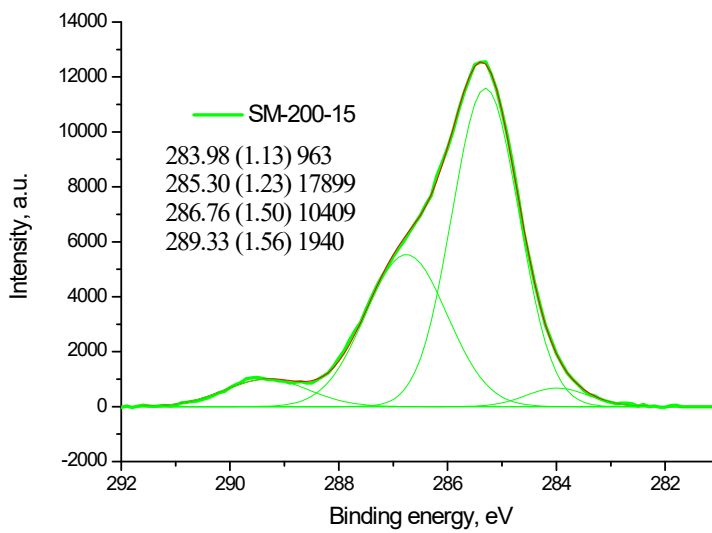
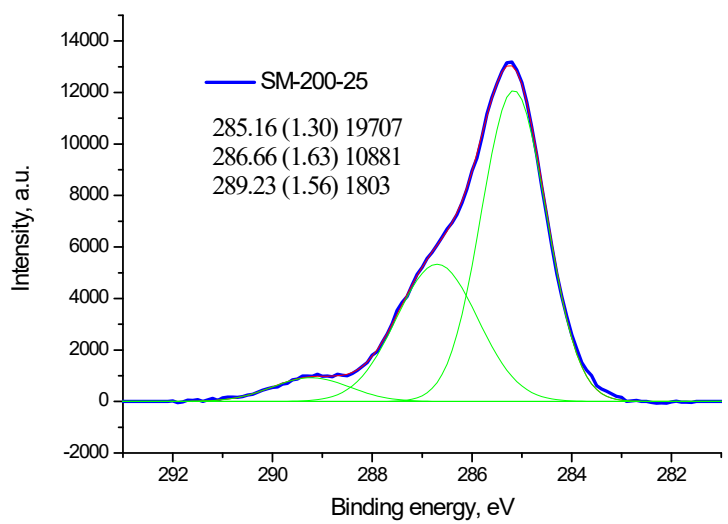


Figure S56 The C 1s photoelectron spectra of SM-200-15, SM-200-25

5. References

- [1] R.P. Vasquez, CuCl by XPS, *Surf. Sci. Spectra.* 2 (1993) 138–143. <https://doi.org/10.1116/1.1247732>.
- [2] G. Moretti, H.P. Beck, Relationship between the Auger parameter and the ground state valence charge of the core-ionized atom: The case of Cu(I) and Cu (II) compounds, *Surf. Interface Anal.* 51 (2019) 1359–1370. <https://doi.org/10.1002/sia.6704>.
- [3] R.P. Vasquez, Cu₂O by XPS, *Surf. Sci. Spectra.* 5 (1998) 257–261. <https://doi.org/10.1116/1.1247881>.
- [4] M. Shima, K. Tsutsumi, A. Tanaka, H. Onodera, M. Tanemura, Chemical state analysis using Auger parameters for XPS spectrum curve fitted with standard Auger spectra, *Surf. Interface Anal.* 50 (2018) 1187–1190. <https://doi.org/10.1002/sia.6414>.
- [5] Y. Mao, J. He, X. Sun, W. Li, X. Lu, J. Gan, Z. Liu, L. Gong, J. Chen, P. Liu, Y. Tong, Electrochemical synthesis of hierarchical Cu₂O stars with enhanced photoelectrochemical properties, *Electrochim. Acta.* 62 (2012) 1–7. <https://doi.org/10.1016/j.electacta.2011.10.106>.
- [6] A.C. Miller, G.W. Simmons, Copper by XPS, *Surf. Sci. Spectra.* 2 (1993) 55–60. <https://doi.org/10.1116/1.1247725>.
- [7] R.P. Vasquez, Cu(OH)₂ by XPS, *Surf. Sci. Spectra.* 5 (1998) 267–272. <https://doi.org/10.1116/1.1247883>.
- [8] R.P. Vasquez, CuCl₂ by XPS, *Surf. Sci. Spectra.* 2 (1993) 160–164. <https://doi.org/10.1116/1.1247736>.
- [9] R.P. Vasquez, CuO by XPS, *Surf. Sci. Spectra.* 5 (1998) 262–266. <https://doi.org/10.1116/1.1247882>.
- [10] J.F. Moulder, W.F. Stickle, P.E. Sobol, K.D. Bomben, *Handbook of X-ray Photoelectron Spectroscopy*, Published by Perkin-Elmer Corporation Physical Electronics Division 6509 Flying Cloud Drive Eden Prairie, MinnCSOla 55344 United Stales of America, 1992. <https://doi.org/10.1002/sia.740030412>.
- [11] M.C. Biesinger, L.W.M. Lau, A.R. Gerson, R.S.C. Smart, Resolving surface chemical states in XPS analysis of first row transition metals, oxides and hydroxides: Sc, Ti, V, Cu and Zn, *Appl. Surf. Sci.* 257 (2010) 887–898. <https://doi.org/10.1016/j.apsusc.2010.07.086>.
- [12] J.P. Espinós, J. Morales, A. Barranco, A. Caballero, J.P. Holgado, A.R. González-Elipe, Interface Effects for Cu, CuO, and Cu₂O Deposited on SiO₂ and ZrO₂. XPS Determination of the Valence State of Copper in Cu/SiO₂ and Cu/ZrO₂ Catalysts, *J. Phys. Chem. B.* 106 (2002) 6921–6929. <https://doi.org/10.1021/jp014618m>.

- [13] D. Dhakal, T. Waechtler, S.E. Schulz, T. Gessner, H. Lang, R. Mothes, A. Tuchscherer, Surface chemistry of a Cu(I) beta-diketonate precursor and the atomic layer deposition of Cu₂O on SiO₂ studied by x-ray photoelectron spectroscopy, *J. Vac. Sci. Technol. A Vacuum, Surfaces, Film.* 32 (2014) 041505. <https://doi.org/10.1116/1.4878815>.
- [14] R.E. Kirby, E.L. Garwin, F.K. King, A.R. Nyairesh, Surface properties of Cr₂O₃, *J. Appl. Phys.* 62 (1987) 1400–1405. <https://doi.org/10.1063/1.339644>.
- [15] G.C. Allen, M.T. Curtis, A.J. Hooper, P.M. Tucker, X-Ray photoelectron spectroscopy of chromium–oxygen systems, *J. Chem. Soc., Dalton Trans.* (1973) 1675–1683. <https://doi.org/10.1039/DT9730001675>.